PERGAMON

Deep-Sea Research II 45 (1998) 1411–1442

DEEP-SEA RESEARCH
PART II

Upper-ocean water mass characteristics of the California current, Summer 1993

A. Huyer*, J.A. Barth, P.M. Kosro, R.K. Shearman, R.L. Smith

College of Oceanic and Atmospheric Sciences, Oregon State University, Corvallis, OR 97331-5503, USA

Received 1 May 1997; received in revised form 3 December 1997; accepted 4 December 1997

Abstract

Two large, high-resolution upper-ocean surveys of the California Current region were conducted in the summer of 1993. Temperature and salinity were measured from a Seasoar vehicle, and velocity was measured by a ship-borne acoustic Doppler current profiler. Both surveys extended from the continental margin to 128°W, and consisted of zonal sections 28 km apart. The first survey (7–28 June) extended from 39.5°N to 36.25°N, and the second (16 August to 1 September) extended from 39.0°N to 37.0°N. The current field was fairly simple in June, showing an equatorward surface jet with only one gentle meander, a nearly continuous poleward California Undercurrent near the continental margin, and two anticyclonic subsurface eddies offshore of the jet. By August meanders in the surface jet had strengthened, and eddies dominated the flow field. Large-scale trends in the water-mass characteristics ("spiciness") along three isopycnal surfaces (26.4, 26.0 and 25.6 kg m^{-3}) show that temperature and salinity tend to increase towards the equator and towards shore, consistent with poleward advection along the continental margin. Local minima in spiciness tend to coincide with the equatorward surface jet. Local maxima in spiciness are associated with subsurface anticyclonic eddies which have a core depth of about 150 m, and seem to originate in the California Undercurrent over the continental slope at local latitudes. We identified several different anticyclonic eddies, each with different water-mass characteristics; all of the eddies we observed had diameters larger than the baroclinic radius of deformation. Water-mass characteristics and migration rates are consistent with formation over the continental margin within the preceding 6–8 months. © 1998 Elsevier Science Ltd. All rights reserved.

1. Introduction

In the last decade or so, there has been increasing evidence that the classical view of the California current as a very broad (> 1000 km) and weak (~ 10 cm s^{-1}) equatorward flow (Wooster and Reid, 1963; Hickey, 1979) can be quite misleading. Instead of a broad weak current, the recent synoptic surveys have shown an intense

*Corresponding author. ahuyer@oce.orst.edu.

0967-0645/98/$ – see front matter © 1998 Elsevier Science Ltd. All rights reserved.
PII: S0967-0645(98)00038-1

equatorward-tending jet with core velocities of 50–80 cm s^{-1} lying offshore of the California continental margin during much of the upwelling season (Kosro and Huyer, 1986; Chelton et al., 1987; Kosro et al., 1991; Strub et al., 1991). Mesoscale CTD and ADCP surveys have indicated that the jet has meanders with a typical curvature radius of > 50 km (Kosro et al., 1991); these meanders seem to grow and migrate due to inherent instabilities (Pierce et al., 1991; Walstad et al., 1991), and occasionally pinch off to form eddies (Strub et al., 1991). There are indications that some eddies have their origin in the California Undercurrent that flows poleward along the continental margin (Kosro et al., 1991; Simpson and Lynn, 1990; Huyer et al., 1984). Prior to 1993, however, there had not been any large synoptic surveys with mesoscale resolution, and many questions remained about the continuity and nature of the jet and the undercurrent, the associated water-mass distributions, and their relation to mesoscale eddies.

During the upwelling season of 1993, two surveys of the California Current were made as part of the ONR-sponsored Eastern Boundary Currents project. The first survey was made during 7–28 June, the second during 28 August–1 September. Both surveys were conducted from the R/V Wecoma; an undulating Seasoar vehicle and a shipborne acoustic Doppler current profiler (ADCP) were the primary sampling tools; the Seasoar vehicle was equipped with a conductivity–temperature–depth (CTD) system and additional instruments for biological sampling. The sampling pattern consisted of long zonal sections extending from the continental margin to 128°W; zonal sections were separated by 28 km and the surveys spanned two or three degrees of latitude (39°30′N to 36°15′N in June, 39°N to 37°N in August). The areal extent is comparable to the coarsely sampled historical surveys conducted by California Cooperative Fisheries Investigations (CalCOFI; Wyllie, 1966) while the horizontal resolution is comparable to the mesoscale surveys made during the 1981–1982 Coastal Ocean Dynamics Experiment (Kosro and Huyer, 1986) and the 1987–1988 Coastal Transition Zone studies (Kosro et al., 1991; Huyer et al, 1991). These are the first surveys that cover a large area of the California Current region with the mesoscale resolution required to resolve the structure of jets and eddies.

These surveys provide a unique opportunity to study the California Current region. In this paper, we examine the subsurface water properties along isopycnal surfaces; in addition to a zonal trend, we find strong local anomalies that are associated with two warm-core eddies. The remainder of this paper is organized as follows: Section 2 provides a brief overview of our sampling methods; Section 3 summarizes our analysis methods, including the choice of isopycnal surfaces; Section 4 describes water-mass and velocity distributions on selected isopycnals; Section 5 further discusses the local anomalies, particularly the two warm-core eddies; and Section 6 contains a brief summary and major conclusions.

2. Sampling and analysis methods

2.1. Seasoar CTD and ADCP sampling

We used a Seasoar vehicle on a 600 m faired cable and a shipborne ADCP to survey the upper ocean off northern California while underway at a speed of about 8 kn

(4 m s^{-1}). The surveys were intended to provide nearly synoptic coverage with mesoscale horizontal resolution over a large area of the California Current, and to operate as continuously as possible in rough seas generated by persistent northwesterly winds. We therefore chose to make long, closely spaced, zonal sections, extending from the continental margin offshore to 128 W. Adjacent sections were separated by a quarter of a degree of latitude (28 km), equivalent to the local internal Rossby radius of deformation. Total duration of each survey was three weeks or less (21 d in June, 16 d in August). The time interval between midpoints of consecutive sections was typically < 30 h. Surveying operations were interrupted occasionally by instrument failure or high seas. We were usually able to operate along the intended ship's heading, but on a few occasions of exceptionally strong winds and heavy seas the ship had to make "dog-leg" approximations to the zonal sections (e.g., on 16–17 June and 24 August, near 37°30′N, 126°30′W).

During both surveys, Seasoar was equipped with an internally mounted SeaBird 9/11*plus* CTD (Kosro et al., 1995), and with an Optical Plankton Counter (Huntley et al., 1995) and a multi-spectral fluorometer (Cowles et al., 1994). The longest Seasoar tows had a duration of ~ 7 d. The tow cable had to be reterminated after most tows, and was gradually shortened. Typical towing speed was 7–8 kn (4 m s^{-1}), and typical cycling time was 9 min, resulting in a horizontal resolution of < 3 km along the ship's track (Fig. 1). Minimum sampling depth was usually < 10 m, and rarely > 25 m. Maximum sampling depths were almost always > 300 m during the June survey. During the August survey, when the tow cable was substantially shorter, maximum sampling depths were usually > 240 m and almost always > 200 m. The Seasoar data were processed by removing the lag between the 24 Hz conductivity and temperature data, by applying conductivity calibrations determined from in situ measurements, by correcting for the thermal mass of the conductivity cell, and by block averaging to 4 Hz values which were sorted and averaged into 2-dbar values for each ascending or descending profile (Kosro et al., 1995). Data from both ascending and descending profiles appear to be of high quality, and are estimated to be accurate to ± 0.01°C in temperature, ± 0.01 psu in salinity, and ± 1 dbar in pressure.

Upper-ocean currents were measured along the ship's track with a 150 kHz, RD Instruments acoustic Doppler current profiler (ADCP). Average profiles of relative velocity between the ship and the ocean were obtained once every 2.5 min. The nominal depth range was 350 m with a pulse length of 12 m (18.8 ms) and a vertical bin width of 8 m (12.6 ms). The shallowest level to yield reliable data was about 25 m. Filter skew and noise bias errors (Chereskin et al., 1989) were estimated to be small (< 1 cm s^{-1}). Navigation data from a GPS receiver were recorded and combined with the relative velocity (vertically averaged across a reference layer) to calculate the ship's velocity and absolute currents. Alignment errors between the transducer and the ship's gyro compass were identified and corrected using methods described by Kosro (1985) and Pollard and Read (1989). The absolute currents were low-pass filtered to suppress signals with periods less than 30 min. For zonal sections, the processed data were interpolated vertically to 10 m intervals and averaged horizontally in 3.2 km bins. For maps of the currents at constant depth (Figs. 1 and 2), the processed data were interpolated vertically to the nominal depth and averaged horizontally in 7.5 km bins.

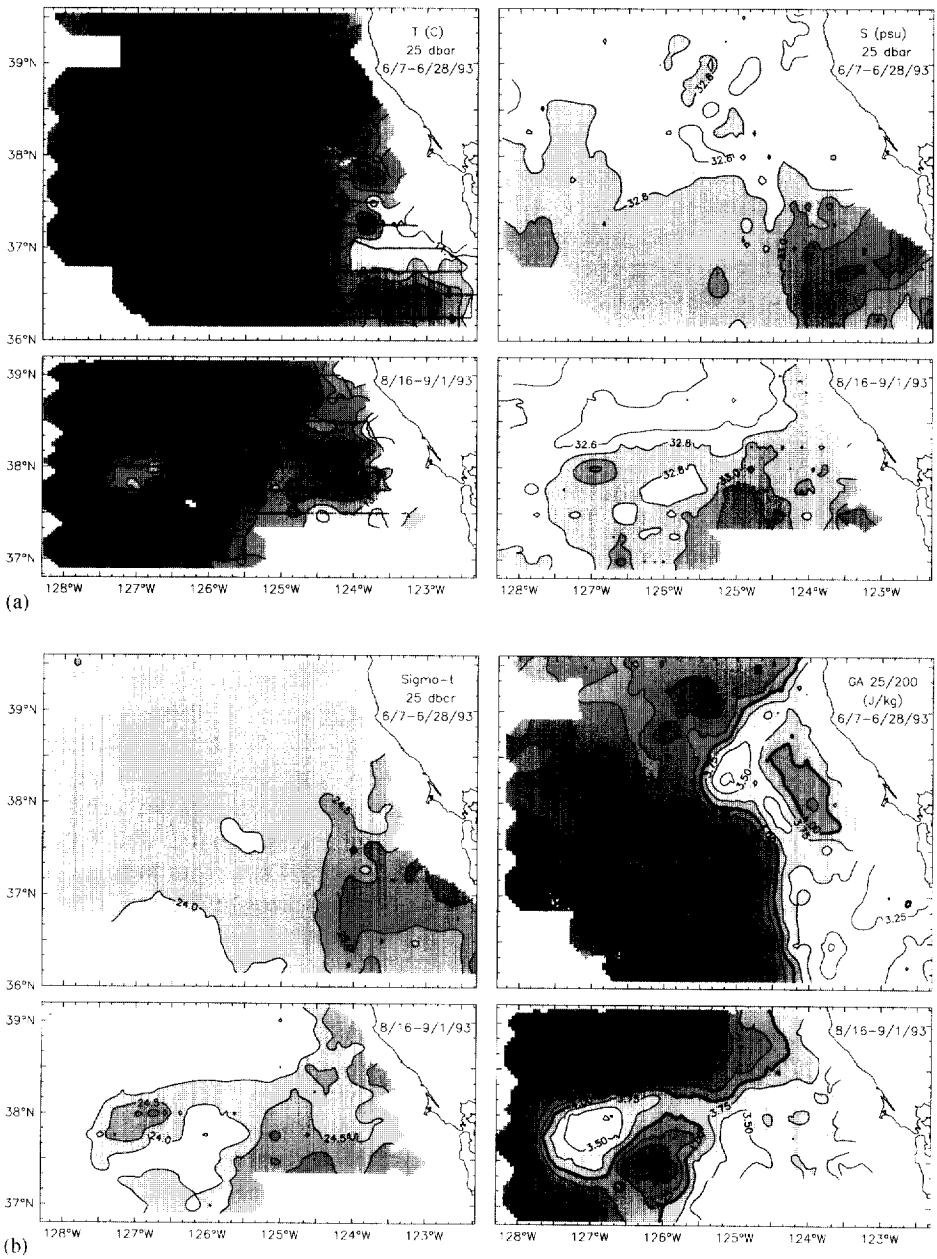

Fig. 1. Near-surface (25 dbar) properties during 7–28 June 1993, and 16 August to 1 September 1993. (a) Temperature (left) and salinity (right); small dots in panels at left show locations of observations. (b) Density (left) and geopotential anomaly relative to 200 dbar (right). (c) ADCP current vectors with superimposed bottom contours (left), and the streamfunction (right) obtained from objective mapping of the ADCP data.

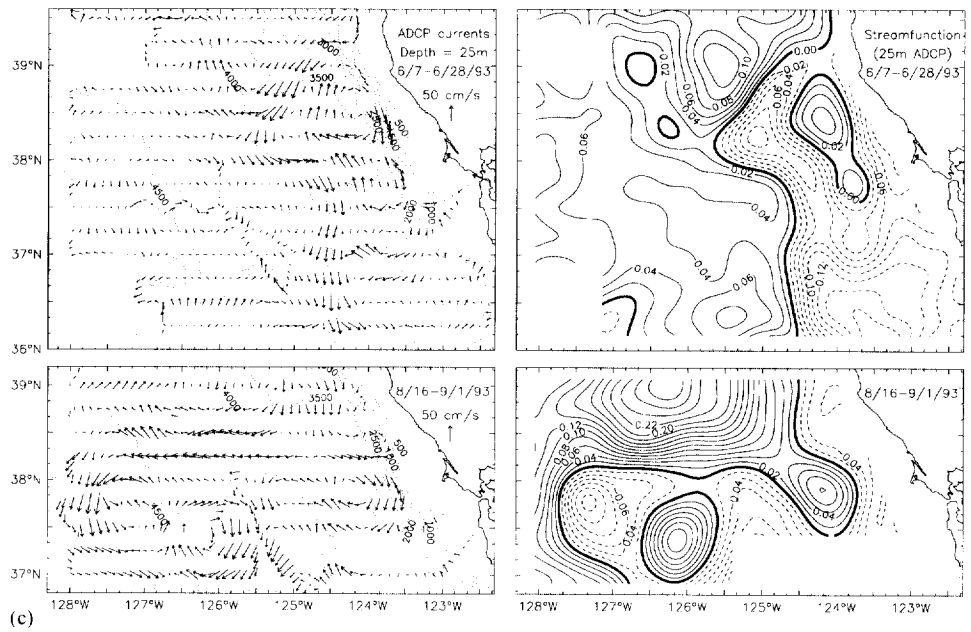

Fig. 1. Continued.

2.2. *Analysis methods*

From the Seasoar temperature, salinity and pressure data we calculated potential density anomaly (σ_θ) and geopotential anomaly relative to 200 dbar using standard algorithms (Fofonoff and Millard, 1983). Differences between σ_θ and σ_t are negligible ($< 0.01\ \mathrm{kg\,m^{-3}}$) over the depth range of our data set. We also calculated values of "spiciness" (Π) – as defined by Flament (1986); spiciness is approximately perpendicular to density anomaly in the T–S plane (Fig. 3) and is often used for studying water-mass distributions (Simpson and Lynn, 1990; Kosro et al., 1991; Huyer et al., 1991). The spiciness variable is particularly appropriate for the California Current region, in which average T–S curves lie roughly orthogonal to isopycnals (Tibby, 1941).

Average T–S curves were obtained by first regridding the Seasoar data using potential density as the independent variable, with a resolution of $\Delta\sigma_\theta = 0.05\ \mathrm{kg\,m^{-3}}$; then all ascending and descending profiles from the same zonal section were averaged together. Fig. 3 shows that zonally-averaged T–S curves for the long sections near 39°N were nearly indistinguishable, and that these averages did not differ significantly between cruises; thus we calculated a single average T–S curve for the northern region. Zonal averages near 36°N (occupied only in June) were quite different from those near 39°N, but did not differ significantly from each other, and thus we also calculated an average curve for the southern region (Fig. 3). Since these average T–S curves are not strictly parallel to lines of constant spiciness (Fig. 3), vertical sections of

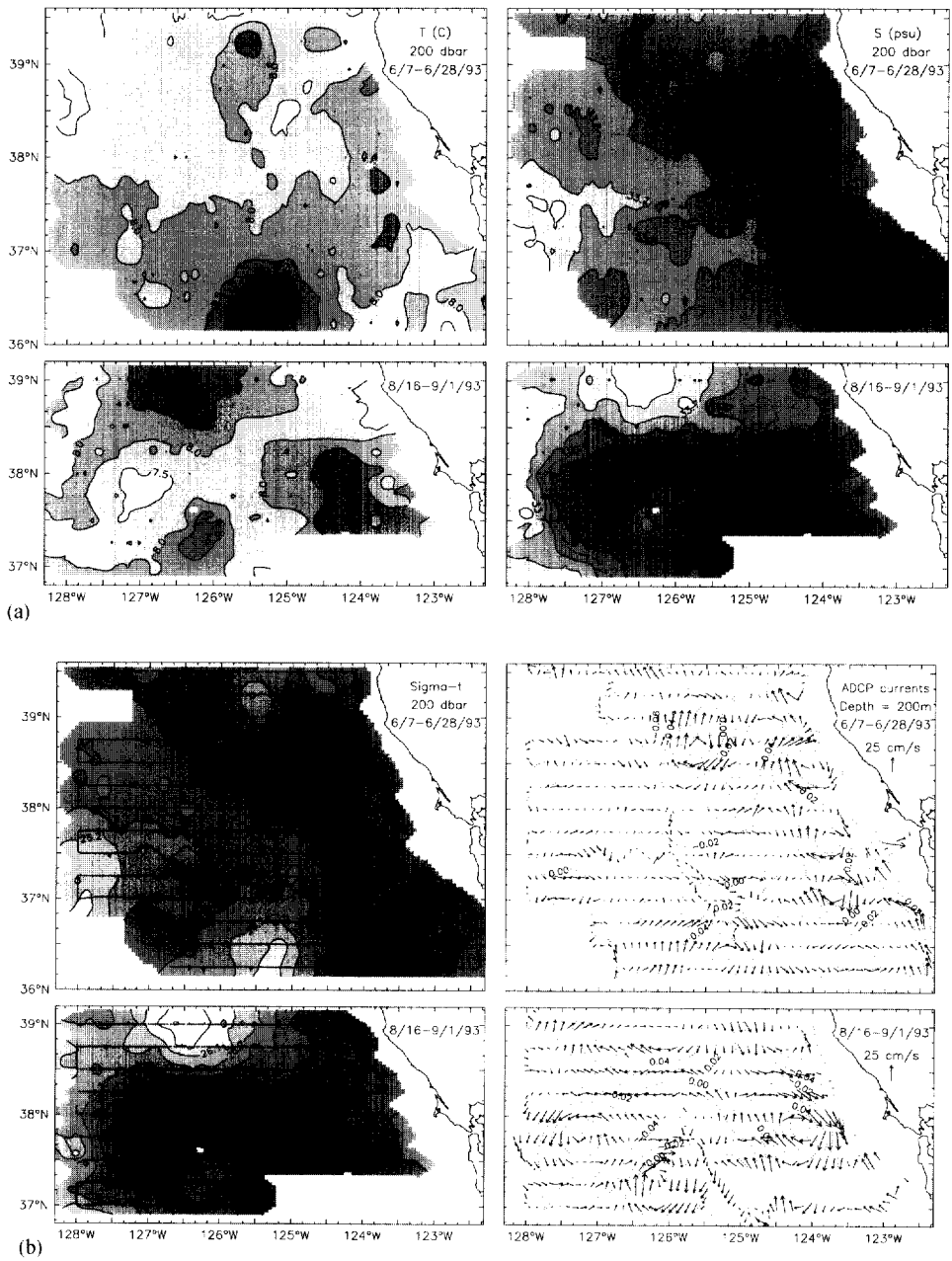

Fig. 2. Sub-surface (200 dbar) properties during 7–28 June 1993, and 16 August to 1 September 1993. (a) Temperature (left) and salinity (right). (b) Density (left) and ADCP current vectors superimposed on the ADCP streamfunction (right).

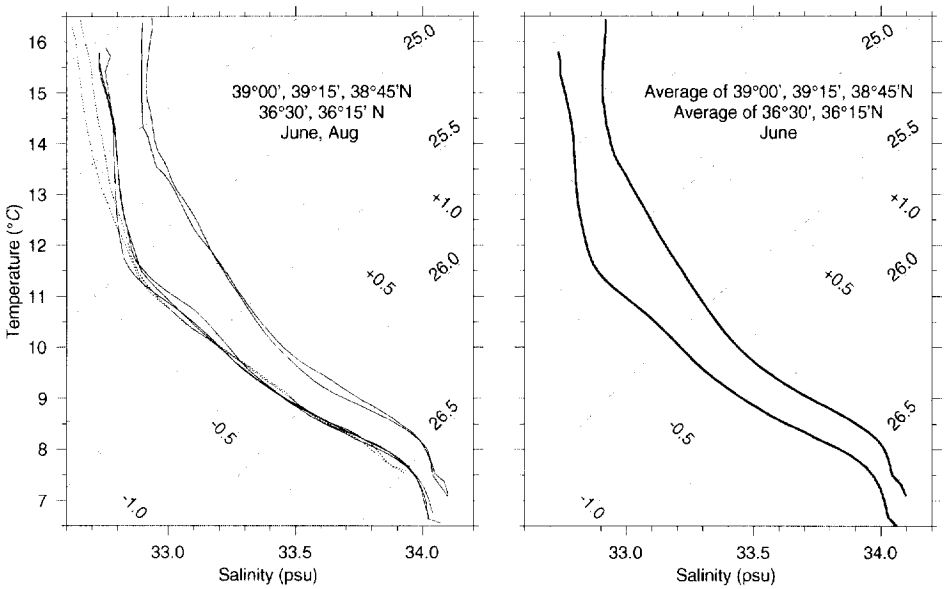

Fig. 3. Average T–S curves for northern and southern portions of the survey area. *Left*: individual zonal sections at 39°15′, 39°00′, 38°45′, 36°30′, 36°15′N in June, and 39°00′, 38°45′ in August (dashed). *Right*: averages of same three northern and two southern sections in June; the northern average lies to the left of the southern average. Curves of constant density (dashed) and constant spiciness (dotted) are superimposed.

spiciness include a background vertical gradient that can obscure anomalous features. Simpson and Lynn (1990) used a "spiciness anomaly" to study an eddy dipole offshore California, and we adopt a similar procedure, i.e. we use spiciness anomalies defined as differences between local spiciness and regionally averaged spiciness to examine the vertical structure of particular features.

To examine the lateral distribution of subsurface water properties, we chose isopycnal rather than isobaric surfaces in order to eliminate noise due to the vertical excursions of internal waves. For each ascending and descending Seasoar profile, the 2 dbar Seasoar CTD data were interpolated vertically to selected isopycnals, specifically $\sigma_t = 26.4\ \mathrm{kg\,m^{-3}}$, $\sigma_t = 26.0\ \mathrm{kg\,m^{-3}}$, and $\sigma_t = 25.6\ \mathrm{kg\,m^{-3}}$. The deepest of these isopycnals ($\sigma_t = 26.4\ \mathrm{kg\,m^{-3}}$) dips down to 240 dbar, the maximum Seasoar sampling depth during the August survey. It reaches this depth in only a few locations, and rises above 140 dbar in a few other locations (Fig. 4); it tends to lie deeper far offshore than inshore. The intermediate isopycnal ($\sigma_t = 26.0\ \mathrm{kg\,m^{-3}}$) lies deeper than 60 m in all but one inshore location (36°55′N, 122°38′W in June), and reaches to depths > 180 m in a few offshore locations (Fig. 5). The shallowest isopycnal ($\sigma_t = 25.6\ \mathrm{kg\,m^{-3}}$) rises from depths > 120 m offshore to depths < 20 m in a few inshore locations along 37°15′N and 37°00′N (Fig. 6).

Current data were interpolated to these isopycnal surfaces by combining the ADCP and Seasoar data for each zonal section. The nominal position of an isopycnal was

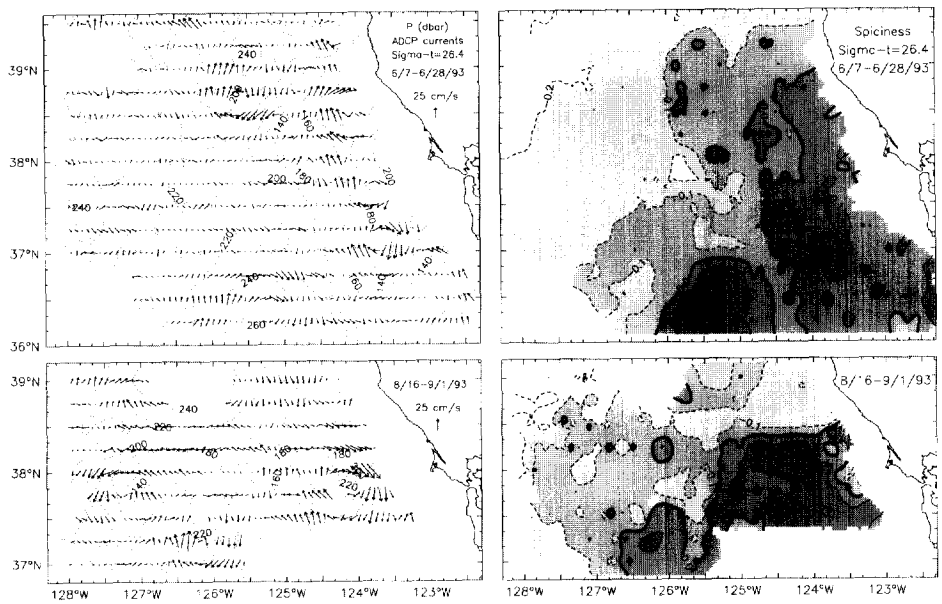

Fig. 4. Properties of the $\sigma_t = 26.4\ \mathrm{kg\,m^{-3}}$ isopycnal: ADCP vectors superimposed on depth contours (left), and spiciness (right).

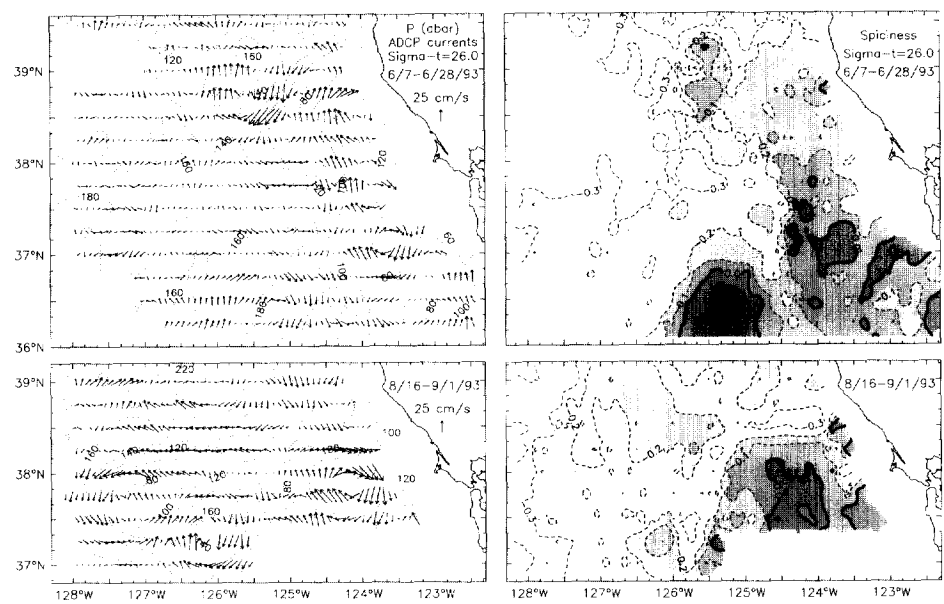

Fig. 5. Properties of the $\sigma_t = 26.0\ \mathrm{kg\,m^{-3}}$ isopycnal: ADCP vectors superimposed on depth contours (left), and spiciness (right).

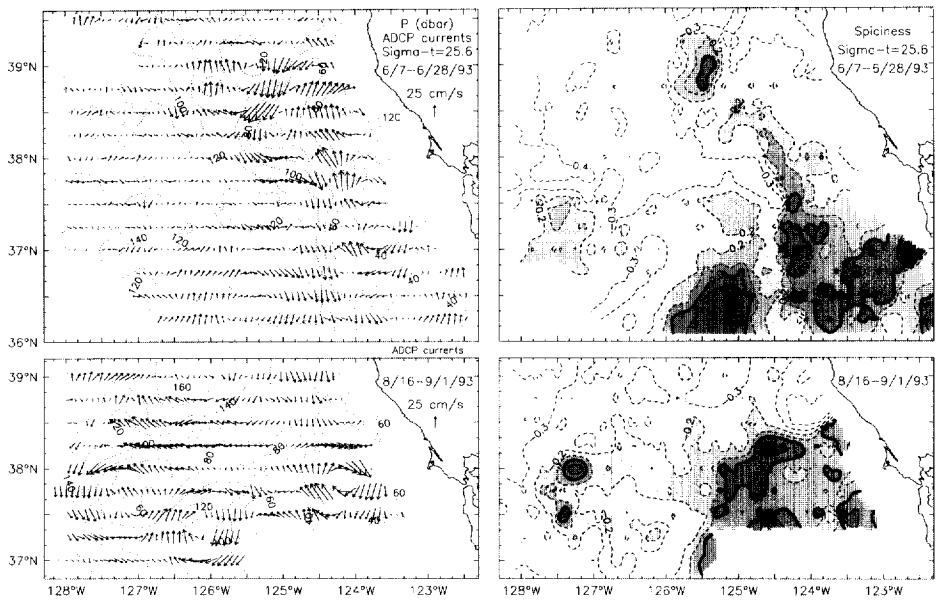

Fig. 6. Properties of the $\sigma_t = 25.6\ \mathrm{kg\,m^{-3}}$ isopycnal: ADCP vectors superimposed on depth contours (left), and spiciness (right).

Table 1
Values of temperature and salinity corresponding to contours of spiciness on selected isopycnals

	Temperature			Salinity		
	$\sigma_t = 25.6$	$\sigma_t = 26.0$	$\sigma_t = 26.4$	$\sigma_t = 25.6$	$\sigma_t = 26.0$	$\sigma_t = 26.4$
$\Pi = -0.2$	10.10	8.87	7.53	33.288	33.544	33.800
$\Pi = -0.1$	10.38	9.18	7.87	33.352	33.607	33.863
$\Pi = 0.0$	10.67	9.48	8.21	33.413	33.671	33.925
$\Pi = 0.1$	10.94	9.78	8.53	33.478	33.734	33.990
$\Pi = 0.2$	11.22	10.07	8.85	33.539	33.798	34.053

taken to be the pressure and location of the nearest 2 dbar Seasoar CTD data point; then the gridded velocity data ($\Delta z = 10$ m, $\Delta x = 3.2$ km) were interpolated vertically and horizontally to this position.

Maps of the T–S characteristics expressed as spiciness are presented for each isopycnal (Figs. 4–6). The contours of spiciness on each isopycnal are parallel to, and can be interpreted as, contours of temperature or salinity: high spiciness corresponds to high temperature or salinity while low spiciness corresponds to low temperature or low salinity (Fig. 3, Table 1). Temperature and salinity (and hence spiciness) on

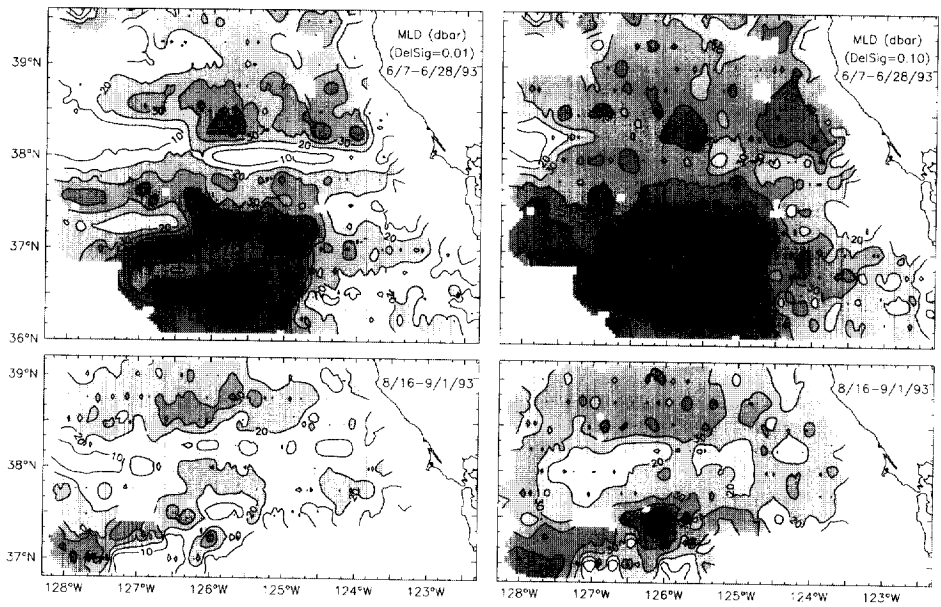

Fig. 7. Distribution of surface mixed layer depth using criteria of $\Delta\sigma_t = 0.01\,\mathrm{kg\,m^{-3}}$ (left) and $\Delta\sigma_t = 0.1\,\mathrm{kg\,m^{-3}}$ (right). The former is a measure of the depth of active surface mixing and thus subject to diurnal variation, while the latter is a measure of the layer that has been recently mixed (Brainerd and Gregg, 1995).

subsurface isopycnals are usually assumed to be conservative: there is no in situ heating and no in situ loss or gain of freshwater. It is usually also assumed that diapycnal mixing is weak compared to isopycnal mixing. However, these assumptions need not be valid in regions where isopycnals approach the surface mixed layer. Mixed-layer depths were generally less than 40 m during both surveys (Fig. 7), and exceeded 50 m only during the June survey and then only in the southwestern quadrant.

3. Results

3.1. Near-surface (25 dbar) fields

The near-surface distributions of geopotential anomaly (at 25 dbar relative to 200 dbar, Fig. 1b) and the directly measured currents (at 25 m, Fig. 1c) show that the flow field in June is dominated by a rather simple and continuous equatorward jet. This jet seemed to cross the continental margin from the shelf to deep water at the northeastern corner of our survey region, and from there flowed nearly straight southward along 124°30′W, with only one large, gentle meander near 38°N. Both the

intensity and the width of the baroclinic flow tended to increase downstream within the survey area; the geostrophic volume transport (through an area 0–200 m deep and 50 km wide centered on the 4.0 J kg^{-1} geostrophic streamline) relative to 200 dbar increased from 1.0 Sv at 39°N to 1.3 Sv at 36.5°N. The southward current is very similar to the meandering jet seen to flow from the shelf-edge at 43°N to a location 200 km offshore at 38°N in June 1987 (Smith, 1992). There is, however, one major difference: the jet seen in June 1987 coincided everywhere with a strong surface density front between warm, fresh oceanic waters and cool, salty, recently upwelled coastal waters (Kosro et al., 1991), but the jet seen in June 1993 did so only in the southern half of our survey region (Fig. 1). This difference can probably be explained by local wind forcing: in both 1987 and 1993, winds in April were strongly favorable for coastal upwelling (Fig. 8), and presumably caused uplift of coastal waters and the formation of a surface density front and associated baroclinic jet within a few days of the onset of favorable winds (Allen, 1973; Huyer, 1990; Allen et al., 1995). In 1987, winds continued predominantly favorable for upwelling in May and June, and the front and jet both migrated far offshore (Kosro et al., 1991). In 1993, however, there was an unusual episode of sustained onshore Ekman transport during the last half of May before strongly favorable winds resumed in June (Fig. 8); these downwelling winds were apparently sufficient to transport warm, fresh offshore surface waters eastward across the jet in the northern half of our survey region. Since the surface layer (20–60 m deep)

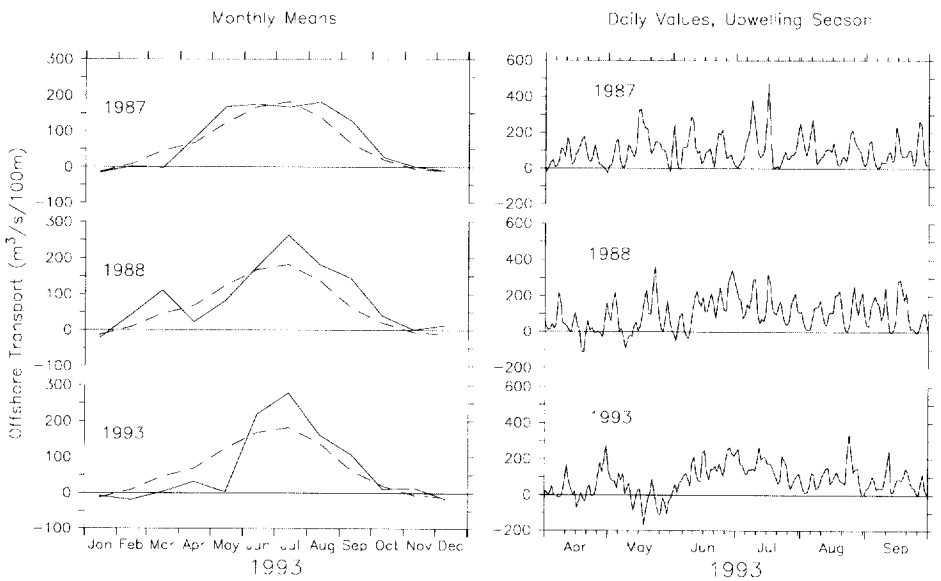

Fig. 8. Monthly (left) and daily (right) values of the offshore component of Ekman transport at 39°N, 125°W, in units of cubic meters per second per 100 m of coastline, calculated from the large-scale atmospheric pressure fields. The dashed line in the panels at left shows the 20-year monthly averages for 1948–1967. (Data provided by NOAA Pacific Fisheries Environmental Group, Pacific Grove, CA).

does not penetrate as deep as the sloping isopycnals (~ 150–200 m, Huyer, 1984; Kosro et al., 1991), such onshore Ekman transport does not completely destroy the jet. Its influence is discernable in the local temperature and salinity minima north of 38°N ($T_{25} < 15$°C, $S_{25} < 32.6$ psu, Fig. 1a) that result from enhanced southward advection along the jet axis (Huyer et al., 1991).

By late August, this relatively simple jet had become quite contorted (Fig. 1b and c), and eddies were obvious both in our survey data and in the trajectories of satellite-tracked drifters drogued at 15 m (Fig. 9; Limeburner et al., 1994; Abbott et al., 1996).

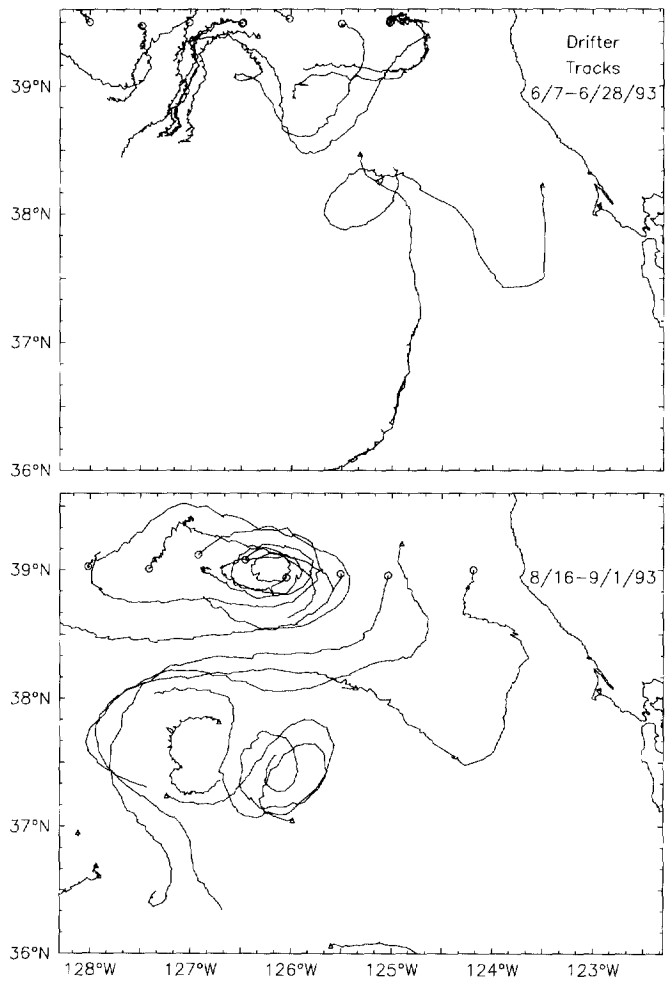

Fig. 9. Trajectories of satellite-tracked drifters during the surveys, from data provided by R. Limeburner (WHOI), M. Abbott (OSU) and J. Paduan (NPS). The beginning of each trajectory is marked by a symbol: a triangle indicates the drifter had been deployed previously, and marks its position at the beginning of the survey period; a small circle marks the location of deployment on 7–8 June or 16–17 August.

Nevertheless, there was a strong tendency for surface waters to be warm and fresh on the offshore (right) side, and to be cold and salty on the inshore (left) side of the current. The surface temperature of offshore waters had increased to $> 17°C$ because of seasonal heating (Nelson and Husby, 1983), and surface salinity of offshore waters had decreased, presumably because of generally southward advection of Subarctic and Columbia River Plume waters (Huyer, 1983). Both processes contribute to a general increase in the geopotential anomaly of offshore waters ($\sim 0.5\,J\,kg^{-1}$ from June to August), and the jet axis now lay approximately along the $4.5\,J\,kg^{-1}$ contour of geopotential anomaly (Fig. 1). Both the distance from the coast and the width of the current (as represented by the separation between the 4.0 and $5.0\,J\,kg^{-1}$ contours) vary on downstream scales of ~ 200 km. The geostrophic transport was about 20% larger than in June. Intervening smaller surveys and satellite images indicate the acute cyclonic meander seen near 37°45′N, 127°15′W in August had evolved from the gentle meander observed near 38°15′N, 125°30′W in mid-June (Kosro et al., 1994; Shearman et al., 1998).

3.2. *Subsurface (200 dbar) fields*

The meandering equatorward flow that is so obvious in the near-surface fields does not penetrate very deep into the water column; it cannot be easily discerned in the 200 m currents in either June or August (Fig. 2b). Nevertheless, the salinity and density fields clearly indicate that the baroclinic shear associated with the equatorward jet does penetrate to 200 m: the $S_{200} = 33.95$ psu contour in June and the $S_{200} = 33.85$ psu contour in August (Fig. 2a) lie directly beneath the axis of the jet (marked by the $\Phi_{25/200} = 4.0\,J\,kg^{-1}$ contour in June and the $\Phi_{25/200} = 4.5\,J\,kg^{-1}$ contour in August, Fig. 1b and c). Similarly the $\sigma_{t-200} = 26.45\,kg\,m^{-3}$ (June) and the $\sigma_{t-200} = 26.35\,kg\,m^{-3}$ (August) density contours lie nearly directly beneath the axis of the surface jet. The positive lateral density gradient across these contours indicates negative geostrophic shear at 200 m.

Inshore of the surface jet, there is a general tendency for zonal density gradients at 200 m to be negative (Fig. 2b), and hence for the shear of the alongshore geostrophic flow to be positive. The directly measured currents (Fig. 2b) show a strong tendency for poleward flow inshore (e.g., near 38°30′N, 124°30′W in June and 37°45′N, 124°40′W in August). This tendency for poleward flow along the continental margin seems to be a manifestation of the California Undercurrent (Huyer et al., 1989, 1991; Collins et al., 1996; Smith et al., 1996a,b) which has its core at a depth of 150–200 m and carries relatively warm, salty waters of more southern origin generally northward (Tibby, 1941; Hickey, 1979; Freitag and Halpern, 1981). Maps of the temperature and salinity at 200 m (Fig. 2a) reflect this generally northward advection along the continental margin.

Other obvious features in the subsurface flow field during the June survey are two anticyclonic eddies lying well offshore of the continental slope: one in the southern portion of the survey region, at about 36°20′N, 125°15′W, and the other in the northern portion, at about 38°35′N, 125°40′W. The southern anticyclonic eddy was centered on a local minimum in density (Fig. 2b), and a local maximum in temperature

(Fig. 2a). At this depth, the southern eddy had a core temperature of $T_{200} > 9.5°C$, a core density of $\sigma_{t-200} < 26.1\ kg\,m^{-3}$, a core spiciness of $\Pi_{200} > 0.1$, azimuthal velocities of $\sim 20\ cm\,s^{-1}$ and a diameter of ~ 100 km. The northern anticyclonic eddy lay near local extrema in both density ($\sigma_{t-200} < 26.3\ kg\,m^{-3}$, Fig. 2b) and temperature ($T_{200} > 8.5°C$, Fig. 2a) at 39°15′N, 125°30′W but was not centered on these extrema, and it did not have a clear spiciness signature at 200 m; azimuthal velocities were $> 20\ cm\,s^{-1}$, and the eddy diameter was ~ 75 km.

The August survey also shows evidence of a northern anticyclonic eddy, centered at about 38°55′N, 126°10′W, on the northern boundary of the survey (Fig. 2). The proximity of this anticyclonic eddy to the position of the northern eddy in June (lying 50 km north-northwest) suggests this is the same eddy, though there are important differences. There is still no spiciness signature, but the core of the northern eddy now coincides with the local minimum in density ($\sigma_{t-200} < 26.0\ kg\,m^{-3}$) which has apparently intensified since June (Fig. 2b); the apparent diameter is larger (> 140 km), and tangential velocities are weaker ($\sim 15\ cm\,s^{-1}$). The August velocity data (Fig. 2b) also shows evidence of a southern anticyclonic eddy centered at about 37°15′N, 126°10′W, which has only a very weak spiciness signature. Unlike the southern anticyclonic eddy in June, this eddy appears to be more intense at the sea surface than at 200 m (cf. Figs 1c and 2b), and it seems to be paired with the strong cyclonic 37°45′N, 127°15′W that had migrated rapidly offshore from 38°15′N, 126°30′W since the June survey (Kosro et al., 1994; Shearman et al., 1998). The August survey did not extend as far south as the June survey, and the subsurface anticyclone observed in June may have persisted through August.

Both June and August surveys also show evidence of an anticyclonic eddy adjacent to the continental slope near San Francisco (Fig. 2b). In August this eddy was rather large (diameter > 80 m) and its center (at 37°50′N, 124°10′W) was clearly seaward of the base of the continental slope, but in June it was just one of a series of small eddies whose centers lay over the outer slope (at 37°35′N, 123°50′W; 37°10′N, 123°40′W; 38°30′N, 124°10′W). These eddies do not seem to have a strong signature in the density field (Fig. 2b), nor in the temperature and salinity fields (Fig. 2a).

3.3. *Isopycnal surfaces*

Distributions of spiciness along three isopycnal surfaces (Figs. 4–6) are used to examine the water properties of the upper ocean. The deepest of these isopycnal surfaces ($\sigma_t = 26.4\ kg\,m^{-3}$) lies deeper than 140 m throughout the entire survey region in both June and August (Fig. 4). This isopycnal has been observed to intersect the sea surface over the inner continental shelf near Pt. Arena during strong coastal upwelling events (Huyer, 1984), but it usually lies deeper than 100 m at the shelf-break. The shallowest isopycnal ($\sigma_t = 25.6\ kg\,m^{-3}$) rises to depths < 40 m of the sea surface at a few locations within our survey area in both June and August (Fig. 6) and its intersection with the sea surface often lies offshore of the shelf-break (Huyer, 1984), and thus temperature and spiciness on this isopycnal need not be conservative at all locations.

The spiciness (Π) distributions for all three isopycnals (Figs. 4–6) show a marked tendency for spiciness (and temperature or salinity, see Table 1) to be higher in the southern and inshore portions of the survey region than in the northern and offshore regions; this tendency is observed in the data from both surveys. The large-scale meridional gradient extends over the full depth range sampled by Seasoar (Fig. 3), and prior work indicates it also extends much deeper (Tibby, 1941; Blanton and Pattullo, 1970). This latitudinal gradient reflects the large-scale oceanographic climate of the eastern Pacific Ocean: high precipitation in the cool subarctic Pacific (Tabata, 1975, 1976) and net evaporation in the warm tropical Pacific (Hastenrath and Lamb, 1977, 1978). The large-scale zonal gradient is associated with net poleward flow along the continental margin, particularly through the California Undercurrent, the California Countercurrent and the seasonal Davidson Current; although these poleward currents vary seasonally and locally (Lynn and Simpson, 1987; Tabata, 1975), the broad water-mass signature is a persistent or recurring feature that has been observed off Southern and central California (Lynn and Simpson, 1987), northern California (Freitag and Halpern, 1981; Huyer et al., 1991), Oregon and Washington (Halpern et al., 1978), and Vancouver Island (Fofonoff and Tabata, 1966). The California Undercurrent is manifested as poleward currents of 10–30 $cm\,s^{-1}$ flowing northward along or near the continental margin (Figs. 4–6). In both June and August, the northernmost sections show poleward flow only on the deepest isopycnal (Fig. 4). In June, the core of the undercurrent separates from the continental slope at about 37°N, and returns to the slope near 39°N: south of 37°N, the strongest northward flow lies inshore of the 2500 m isobath, but between 37° and 38°30′N it lies beyond the 3500 m isobath.

In addition to these large-scale spiciness trends, the distributions of spiciness show some striking mesoscale features. One of these is a region of high spiciness ($\Pi > 0.1$) centered at about 36°20′N, 125°15′W on all three isopycnals in June (Figs. 4–6); it coincides with a region of anticyclonic flow on all three isopycnals, and with a local depression in the depth of the two deeper isopycnals (Figs. 4 and 5). These are all manifestations of the southern anticyclonic eddy identified in Fig. 2. The highest spiciness in the core of this eddy ($\Pi > 0.2$) occurs on the 26.0 isopycnal, at a depth of ~ 180 m (Fig. 5). This value exceeds the spiciness of the immediate surroundings by about 0.4, and it exceeds the spiciness of *all* inshore waters on the same isopycnal by about 0.2 (Fig. 5). Maximum tangential velocities (15–25 $cm\,s^{-1}$) around this eddy coincide approximately with the spiciness contours $\Pi_{26.4} = 0.1$, $\Pi_{26.0} = 0.0$ and $\Pi_{25.6} = -0.1$; all indicate an eddy diameter of ~ 100 km.

A weaker, less coherent spiciness anomaly (with $\Pi_{25.6} > 0.0$) at about 39°00′N, 125°30′W is seen most clearly on the shallowest isopycnal in June (Fig. 6). This lozenge-shaped ($\sim 30 \times 80$ km) spiciness maximum coincides approximately with the northern anticyclonic eddy identified in Fig. 2; maximum tangential velocities of $\sim 15\,cm\,s^{-1}$ coincide approximately with the contours of $\Pi_{26.0} = -0.2$ and $\Pi_{25.6} = -0.2$ (Figs. 5 and 6). The deepest isopycnal shows some very small spiciness maxima in the general vicinity of this eddy in June, but no single coherent core that

coincides with either the pressure maximum (at $P > 220$ m), or the center of rotation (Fig. 4). In August, a very subtle spiciness maximum ($\Pi_{25.6} > -0.2$) at 39°N, 126°30′W coincides with a center of rotation and with the center of a depth depression (> 160 m. Fig. 6); the zonal axis of this feature is ~ 120 km. Perhaps the same lozenge-shaped eddy grew larger and turned sideways, and its narrow core now lay between the zonal sections at 39°00′N and 38°45′N; during both surveys, the longer axis lay parallel to the jet axis, and the turning of the eddy might be associated with the development of the meander in the baroclinic jet.

Even more subtle is the spiciness signature of the baroclinic jet, which can be seen on the shallowest isopycnal as a local minimum under the axis of the jet in June, i.e., at 39°00′N, 125°00′W, at 38°30′N, 125°30′W, and near 124°30′W on each section between 37°30′ and 36°15′N (cf. Figs. 1c and 6); at these locations the current vectors on the isopycnal lie nearly tangential to the axis of the surface jet. In August there are also some isolated spiciness minima that seem to coincide with the jet axis. Several small patches of high spiciness occur in regions where this isopycnal lays relatively close to the surface ($P < 60$ dbar); these include two very small patches ($\Pi_{25.6} > 0.1$ west of 127°W) on the inshore flank of the jet and within a cyclonic meander. Currents in the core of the surface jet are strongly baroclinic: the continuous equatorward current is obvious and quite strong on the 25.6 isopycnal in both June and August (> 15 cm s^{-1} along $P_{25.6} = 80$ dbar; Fig. 6), but it is absent (in June) or barely discernible (< 10 cm s^{-1}, in August) on the 26.4 isopycnal (Fig. 4).

The general tendency of these isopycnals to slope upward toward the coast is due, at least in part, to the seasonal upwelling along the coast. In winter, this tendency is absent. For example, February 1981 CTD sections extending 350 km west along 39°30′N and 350 km southwest from the coast at 38°40′N show that the 26.4 isopycnal lay everywhere at depths of ~ 200 m or more, and that the 26.0 isopycnal lay at depths of 125–175 m, both inshore and offshore (Fleischbein et al., 1981). In both June and August, the 26.4 isopycnal surface rose generally up toward the east from depths > 220 m at locations far offshore (e.g. at 37°N, 128°W) to depths of 160 m along the continental margin (Fig. 4). Shallowest depths lay generally along a ridge ~ 20 km inshore of the axis of the surface jet (cf. Fig. 1b and c). Inshore of the ridge, current vectors were generally poleward and the isopycnal tilted generally downward toward the east, implying positive geostrophic shear and suggesting that the core of the poleward California Undercurrent lay above this isopycnal surface; a core-depth of ~ 175 m has been tentatively confirmed by moorings (Kosro et al.,1996) and by ship-borne ADCP surveys (Smith et al., 1996a). A local minimum in the depth of this isopycnal (< 140 m at 38°25′N 125°00′W in June and at 37°55′N 127°00′W in August) coincides with counterclockwise flow (Fig. 4) and seems to represent a cyclonic eddy that formed over the continental slope in May 1993 (Chumbinho, 1994; Kosro et al., 1994). Local depth maxima (> 220 m) are associated with clockwise flow and represent the anticyclonic eddies identified in Fig. 2. The 26.0 and 25.6 isopycnal surfaces (Figs. 5 and 6) have very nearly the same shape as the 26.4 kg m^{-3} surface (Fig. 4), and lie shallower by about 60 and 90 m, respectively.

4. Discussion

The most striking mesoscale features in the spiciness distributions are the local maxima that are associated with anticyclonic circulation. We turn now to a more detailed examination of these features to learn more about their essential nature and characteristics.

4.1. The southern subsurface warm-core eddy

The southern subsurface warm-core feature centered at about 36°20′N, 125°15′W was a dominant spiciness signal on all three isopycnals in June (Figs. 4–6). Unless it underwent radical transformation and northwestward migration to 37°30′N, 126°10′W, this feature was not observed in August. In June, its signature was absent or very weak at the sea surface: there is no hint of it in the 25 dbar water properties (Fig. 1a), nor in the geopotential anomaly (Fig. 1b), but there is a suggestion of anticyclonic flow in the 25 m ADCP data (Fig. 1c). At deeper levels, its signature is robust: at 200 m, the core is > 1°C warmer and 0.2 kg m^{-3} lighter than ambient waters and tangential velocities around the core are > 20 cm s^{-1} (Fig. 2a and b). Anticyclonic tangential velocities are observed on all three isopycnals, which span a depth range of 120–260 m at the core (Figs. 4–6).

Vertical sections (Fig. 10) provide clear evidence that this eddy has a subsurface core. Zonal distributions of spiciness anomaly show a lens of high spiciness ($\Delta\Pi > 0.1$) about 200 m thick and 90 km across at 36°15′N, and about 150 m thick and 70 km across at 36°30′N; on both sections, the lens is centered at a depth of 150 m and 125°15′W. The T–S anomalies are remarkably uniform over a wide density range within the lens, especially along 36°15′N (Fig. 11). Isopycnals diverge away from the core of the lens, both above and below; the perturbation in the density field extends up to ~ 70 m and down to > 300 m (Fig. 10). The sense of the horizontal density gradients implies that the geostrophic component of the anticyclonic circulation has its maximum speed at a depth of ~ 150 m. The ADCP data from 36°30′N show a region of strong northward flow ($v \sim 20$ cm s^{-1}) just west of the high-spiciness lens, a region of strong southward flow ($v \sim -20$ cm s^{-1}) just east of it, and net zonal flow ($u \sim 10$ cm s^{-1}) within it; this combination implies the center of the eddy lies south of this line. The ADCP data from 36°15′N also show strong meridional currents on either side of the lens ($v < -20$ cm s^{-1} at 120–150 m near 125°00′W and $v \sim 20$ cm s^{-1} at 110–160 m near 126°00′W); the zonal flow here is very weak ($|u| < 10$ cm s^{-1} at 100–200 m from 124°45′ to 126°15′W). The velocity minimum on this section lies at about 125°30′W, about 25 km west of the center of the lens. Using the approximation of a circular eddy centered at 36°15′N, 125°30′W, we can plot tangential velocity vs. radial distance (Fig. 12) to estimate eddy size and angular velocity; in the layer between 120 and 180 m, the angular velocity is approximately constant at 0.45 day^{-1} within 50 km of the center; a full rotation takes about 14 d. At depths of 220–260 m, below the core, the water column rotates more slowly (once in 24 d), and over a larger radius (60 km).

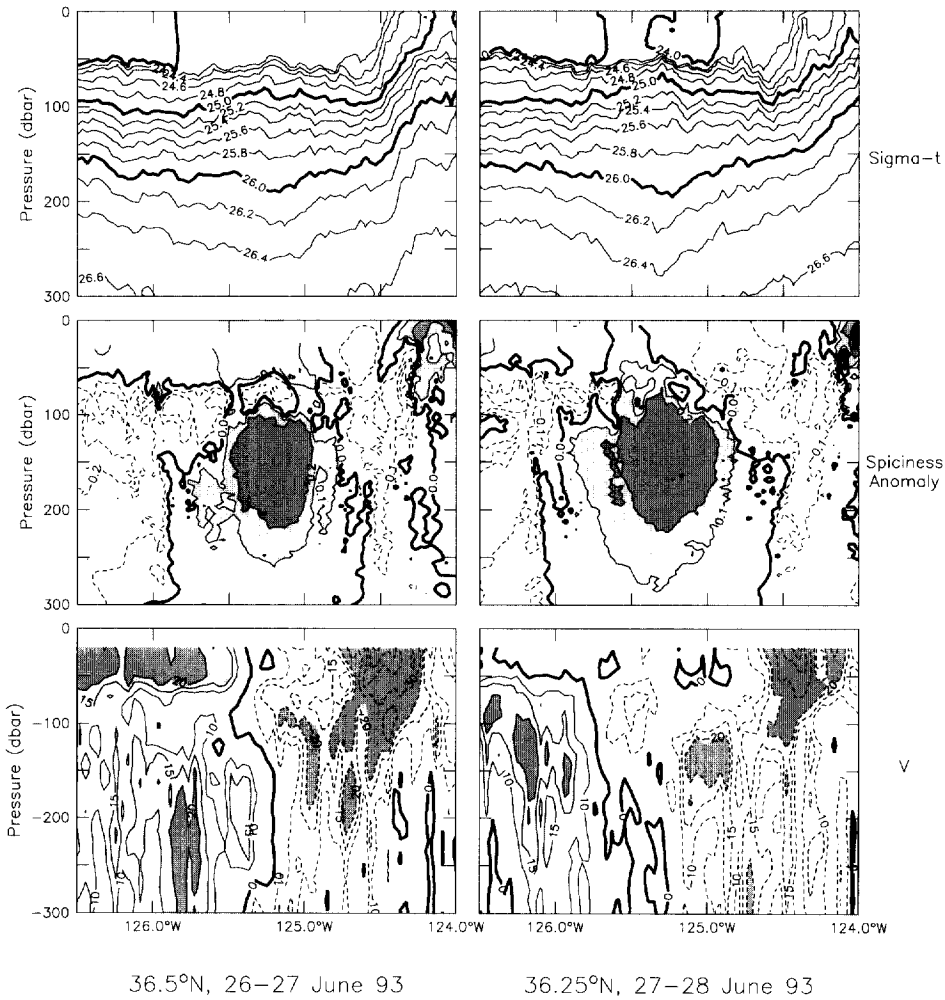

Fig. 10. Zonal sections through the southern subsurface warm-core eddy: density, spiciness anomaly and the northward component of velocity, along 36°15′N and 36°30′N, 26–28 June 1993. (Spiciness anomaly is the difference between the actual spiciness and the southern average shown in Fig. 3).

In contrast to the lateral homogeneity of the interior of the high-spiciness lens, water properties on its flanks are very heterogeneous (Fig. 13). Lateral scales of the anomalies from a smooth gradient range from < 5 to ~ 15 km; the ADCP data shows current variations of $\pm 5\,\mathrm{cm\,s^{-1}}$ over similar scales (Fig. 13). Many of the small water-mass anomalies on the flanks of the lens are coherent across isopycnals, over density ranges of $\sim 0.5\,\mathrm{kg\,m^{-3}}$, and this coherence is often oblique rather than strictly vertical. Such complex fine-scale structure on the flanks of the lens could result

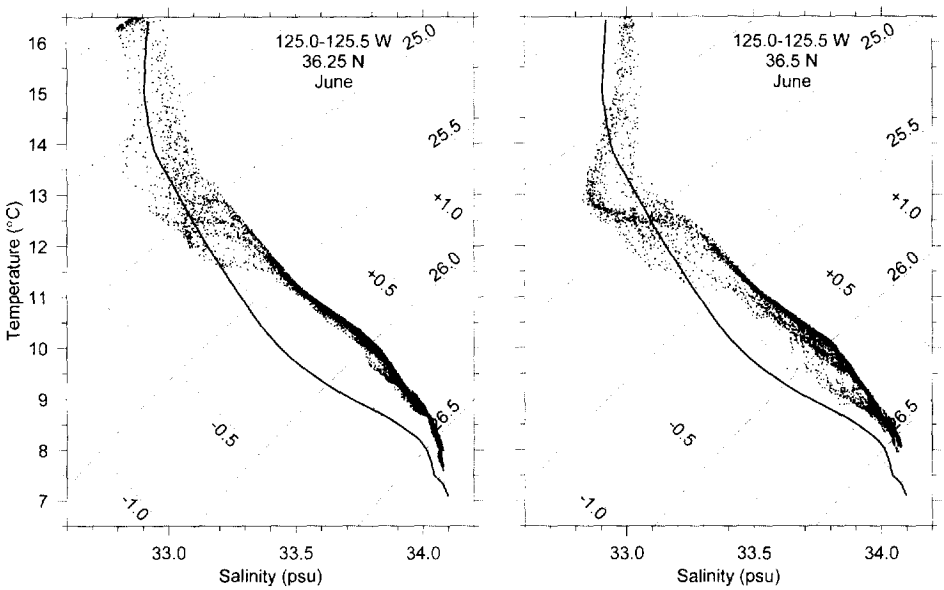

Fig. 11. T–S diagrams of Seasoar data near the core of the southern subsurface warm-core eddy. The southern average from Fig. 3 is repeated for reference.

from stirring by laterally sheared internal waves and other submesoscale processes superimposed on the mesoscale fields.

Given the large-scale water mass gradients in this region, this lens must have originated inshore and/or farther south. The core-depth of about 150 m coincides with the core of the California Undercurrent, and suggests the eddy likely formed inshore from a meander in the Undercurrent; recent float data suggests that the Undercurrent sheds eddies intermittently (Garfield et al., 1998). The spiciness values ($\Pi \sim 0.16$) at the core of the lens exceed any observed inshore during either of our surveys (Figs. 4–6) and also exceed those observed anywhere during a high-resolution CTD survey of this region in March 1992 (Lynn et al., 1995). The core T–S characteristics of 10°C, 33.8 psu on the $\sigma_t = 26.0\,\mathrm{kg\,m^{-1}}$ isopycnal (Fig. 11) are as high as those observed on the same isopycnal in the Southern California Bight (Lynn and Simpson, 1990; their Figs. 8–10), and thus it is conceivable that this eddy originated at or near Pt. Conception. Statistics from the recent float data (Garfield et al., 1998), however, indicate this is unlikely. Of 20 floats deployed at depths of about 300 m over the continental slope off San Francisco or Monterey, almost all exhibit three flow patterns: oscillating flow along the continental margin, steady poleward flow in the California Undercurrent, and rotary flow around anticyclonic eddies migrating westward away from the margin at a mean speed of $1.2\,\mathrm{cm\,s^{-1}}$. A subsurface anticyclonic eddy detected at about 37°N, 128°W in May 1992 also showed westward propagation (T. Chereskin, personal communication). Our southern warm-core eddy was observed

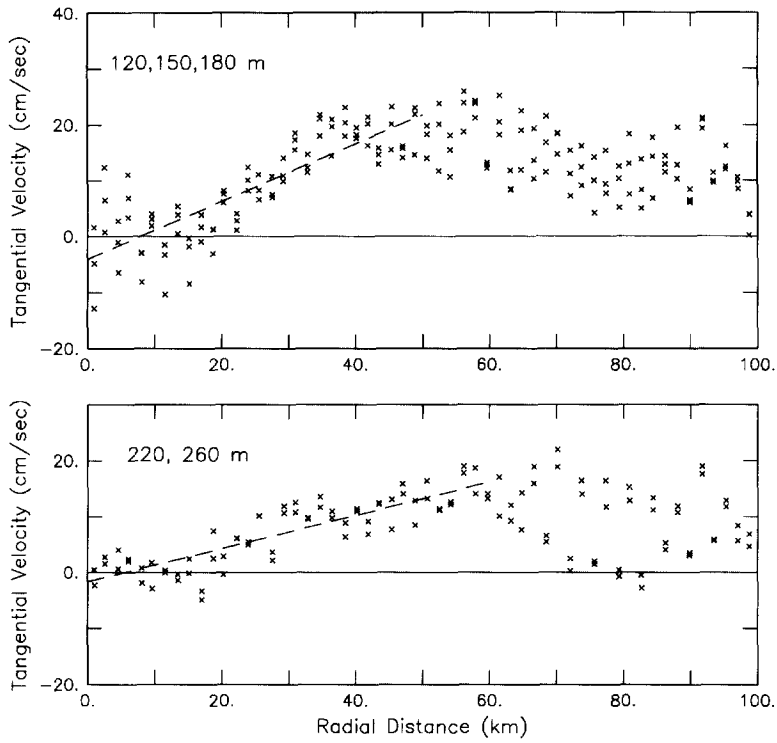

Fig. 12. Tangential velocities versus radial distance, calculated from ADCP data from selected depths along 36°15′N, assuming a circular eddy centered at 36°15′N, 125°30′W; the slope of each regression line corresponds to angular velocity.

about 200 km offshore of the continental margin in late June, and westward migration at 1.2 cm s^{-1} implies it originated over the slope in mid-winter. We do not have CTD data from the continental slope at local latitudes for the winter of 1992–1993, but T–S characteristics from other winters (Fig. 14) are similar to those observed in our southern warm-core eddy.

The basic structure of this subsurface eddy and its probable inshore origin are reminiscent of the high-salinity "meddies" in the eastern North Atlantic, which originate near Cape St. Vincent, Portugal (Armi et al., 1989; Prater and Sanford, 1994). Indeed, Garfield et al. (1998) have already adopted the term "cuddies" for subsurface anticyclonic eddies originating in the California Undercurrent. We note that our southern subsurface warm-core eddy has a larger diameter (by a factor of 2 or 3), shallower core-depth (150 m, cf. 1000 m), smaller thickness, stronger stratification, and more subtle water mass signature than a typical meddy (e.g., Richardson et al., 1989). The eddy core also lies considerably shallower (by $\sim$ 150 m) than the typical depth of the subsurface floats deployed by Garfield et al. (1998).

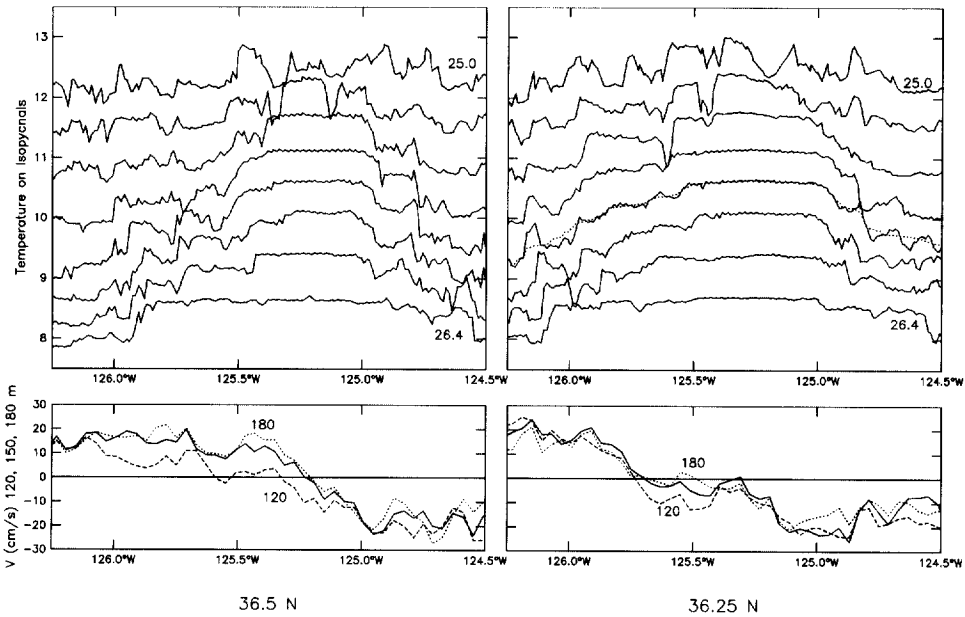

Fig. 13. Lateral profiles of temperature and velocity along the zonal sections at 36°15′ and 36°30′N. Upper panels show temperature on selected isopycnals (25.0–26.4 kg m^{-3} at intervals of 0.2 kg m^{-3}); lower panels show the northward current at 120, 150 and 180 m.

4.2. *The northern warm-core eddy*

A subsurface anticyclonic eddy was also observed near the northern boundary of our survey region, in both June and August (Fig. 6). In June, the entire eddy lay within our survey region, but in August we sampled only the southern half of the eddy. Between the two surveys, the eddy center moved westward from about 39°00′N, 125°30′W to about 39°00′N, 126°30′W, a distance of about 85 km in 65 d. This migration rate, 1.5 cm s^{-1}, is very similar to that observed by the subsurface floats trapped in "cuddies" (Garfield et al., 1998). It therefore seems very likely that the two surveys sampled the same eddy. Combining its position in early June with the average migration rate of 1.5 cm s^{-1} suggests the eddy originated over the continental slope in late March or early April.

Like the southern eddy, the northern eddy in June was not discernible in the near-surface water properties (Fig. 1a). Unlike that eddy, however, it has a clear signature in the near-surface velocity fields, both in the dynamic topography and in the ADCP data (Fig. 1b and c): the anticyclonic currents are tangential to the 4.5 J kg^{-1} geostrophic streamline centered at about 39°07′N, 125°30′W. The eastern flank of the eddy is indistinguishable from the offshore flank of the equatorward jet near the surface (Fig. 1c) but the equatorward jet is completely attenuated by 200 m and the anticyclonic eddy remains as a robust feature with tangential velocities of

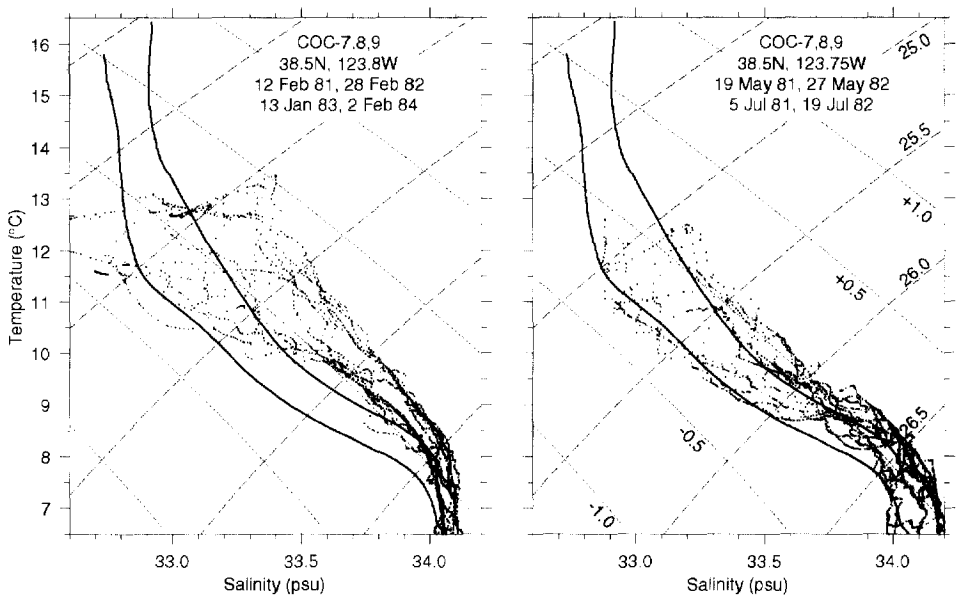

Fig. 14. T–S diagrams of CTD data from three stations over the continental slope on the CODE Central Line, at about 38°30′N. Left panel shows data from four winter sections; right panel shows data from two spring and two summer sections. The regional averages from Fig. 3 are repeated for reference.

$\sim 25\ \mathrm{cm\,s^{-1}}$ (Fig. 2b). At 200 m, waters in the eddy core were > 0.5°C warmer (and $0.2\ \mathrm{kg\,m^{-3}}$ lighter) than its immediate surroundings, but nearly 1°C cooler (and $> 0.1\ \mathrm{kg\,m^{-3}}$ heavier) than the southern warm-core eddy. All three isopycnal surfaces (Figs. 4–6) show a local depth depression near the center of this eddy. The two shallower isopycnals both show a strong spiciness maximum in the eddy core (Figs. 5, and 6), but the deepest isopycnal does not (Fig. 4). The maximum spiciness values in the eddy core ($\Pi > 0.0$ at $\sigma_t = 25.4\ \mathrm{kg\,m^{-3}}$) are generally higher than those elsewhere in our survey region; exceptions occur only within the southern eddy and at shallow depths (< 60 m) where spiciness is not necessarily conserved.

Vertical sections through this eddy in June (Fig. 15) show that the strongest spiciness anomalies and smallest geostrophic shear occur at depths between 100 and 150 m. Unlike the southern eddy, this one has no large lens of uniform spiciness at its core, but instead has a very patchy distribution of generally high values in a column about 80 km across and 200 m deep. Nevertheless, small areas (< 30 km across) of the same spiciness anomaly ($\Delta\Pi \sim 0.35$, at $\sigma_t = 25.5\ \mathrm{kg\,m^{-1}}$) occur on two of the zonal sections that intersect this eddy (Fig. 15). T–S diagrams (Fig. 16) confirm that the water properties of this eddy are much less homogeneous than those of the southern eddy. We speculate that the patchiness of this eddy, compared to the uniformity of the southern anticyclonic eddy, is related to its inferred spring-time formation: results from the Coastal Ocean Dynamics Experiment have shown the isopycnals that lie

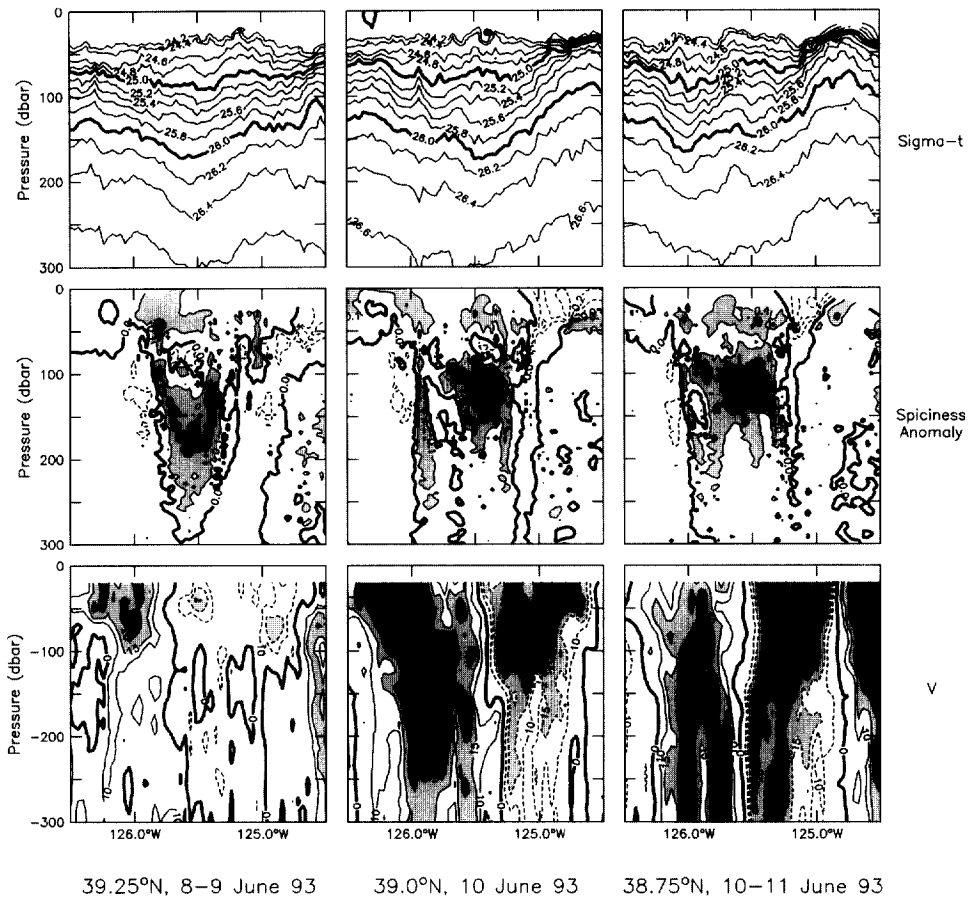

Fig. 15. Zonal sections through the northern warm-core eddy in June: density, spiciness anomaly and the northward component of velocity, along 39°15′N, 39°00′N and 38°45′N, 8–11 June 1993. (Spiciness anomaly is the difference between actual spiciness and the northern average shown in Fig. 3).

near the eddy core are often exposed to the sea surface and surface heat fluxes in early spring: they are intermittently exposed during strong upwelling events and suppressed again during brief downwelling events (Huyer, 1984). In the presence of alongshore inhomogeneities in both the ocean and the atmosphere, such transient exposures are likely to result in lateral patchiness. Such intermittent on/offshore advection is also likely to stir shelf and upper slope waters together, diluting the water mass signature of the California Undercurrent; this scenario is consistent with the seasonal change in slope water characteristics suggested by Fig. 14. In contrast, these same isopycnals lie at depths well below the surface layer in mid-winter (Huyer, 1984), the inferred time of formation of the southern eddy.

The zonal sections at 39°00′N and 38°45′N (Fig. 15) both show maximum meridional velocities of $\sim 30\ \mathrm{cm\ s^{-1}}$ on either side of the high spiciness region, at a distance

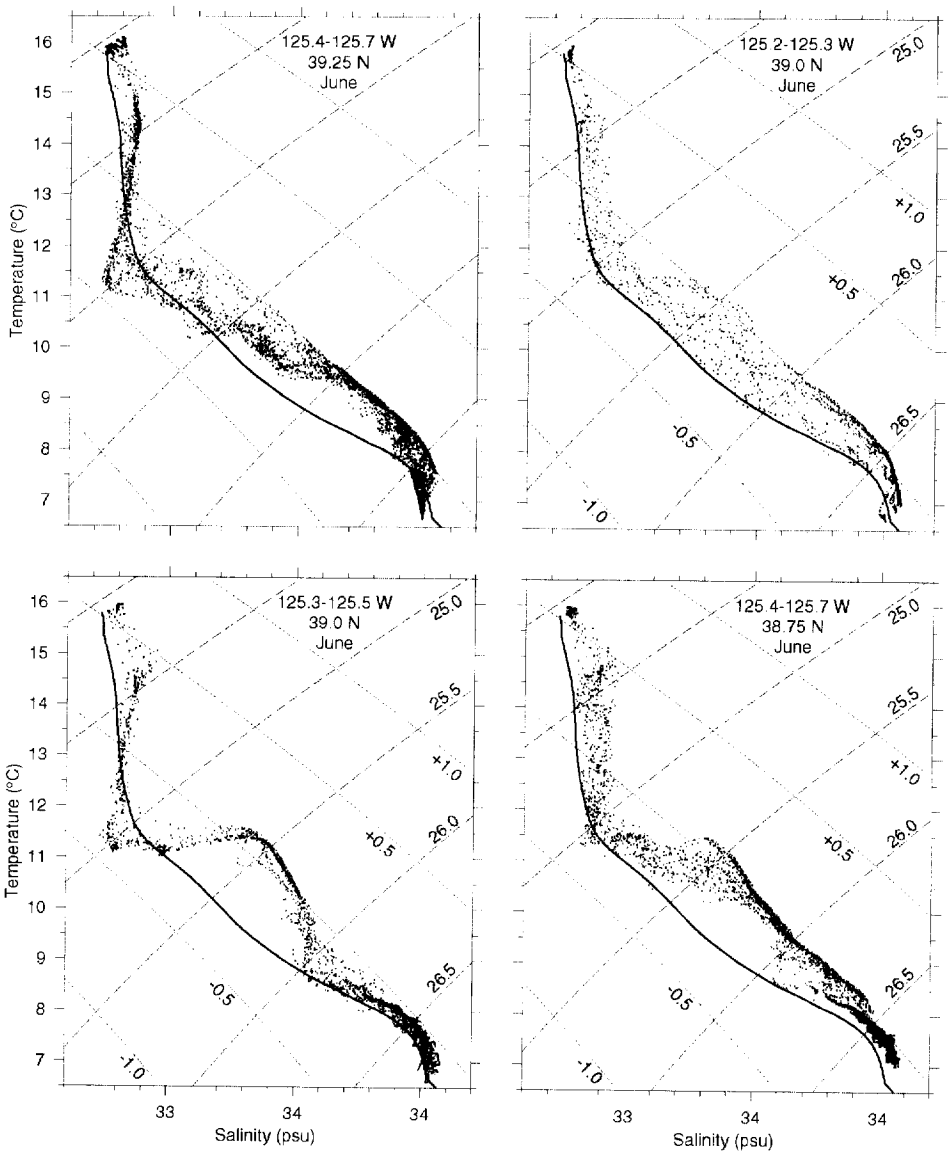

Fig. 16. T–S diagrams of Seasoar data near the core of the northern warm-core eddy in June. The heavy curve in each panel repeats the northern average from Fig. 3.

of $\sim$ 35 km from the eddy center; these would imply a rotation period of $\sim$ 9 d if the eddy were circular. At 39°15′N, there is little meridional flow (Fig. 15), but significant eastward flow ($u \sim 15$ cm s^{-1}) indicates that this line cuts through the northern flank of the eddy; the spiciness anomaly here barely penetrates down to 250 m. Similarly, on

the section at 38°30′N across the southern flank (not shown), there is a band of strong westward flow ($u < -20\ \mathrm{cm\,s^{-1}}$) between 125°25′ and 125°45′W that contains positive spiciness anomalies above 200 m. The vertical shear of the tangential velocity of this eddy is small compared to the shear in the southern subsurface eddy.

Temperature profiles through the northern eddy (Fig. 17) show that its flanks were highly heterogeneous and contain some sharp spiciness anomalies with radial scales of < 10 km. One of these anomalies, at 125°56′W, 39°00′N, has very high vertical coherence (from $\sigma_t < 25.0\ \mathrm{kg\,m^{-1}}$ to $\sigma_t > 26.4\ \mathrm{kg\,m^{-1}}$). A strikingly similar anomaly was observed 25 h later at 126°00′W, 38°45′N; both coincide with northward currents of $\sim 25\ \mathrm{cm\,s^{-1}}$. If these represent two observations of the same small feature, it must have an azimuthal length of at least 50 km.

In August, the northern anticyclonic eddy is much larger (with diameter of ~ 150 km) than it was in June. Its velocity signature extends from the surface (Fig. 1b and c) to a depth of at least 200 m (Fig. 2b). At all depths, the inshore flank of the eddy is indistinguishable from the offshore flank of the jet, which now penetrates to 200 m. Diverging isopycnals across the eddy (Fig. 18) indicate the core of the eddy is now at ~ 100 m, i.e., shallower than it was in June, and the tangential currents are now nearly barotropic, without a clear subsurface maximum. In August, the eddy has no obvious high-spiciness core on any of the

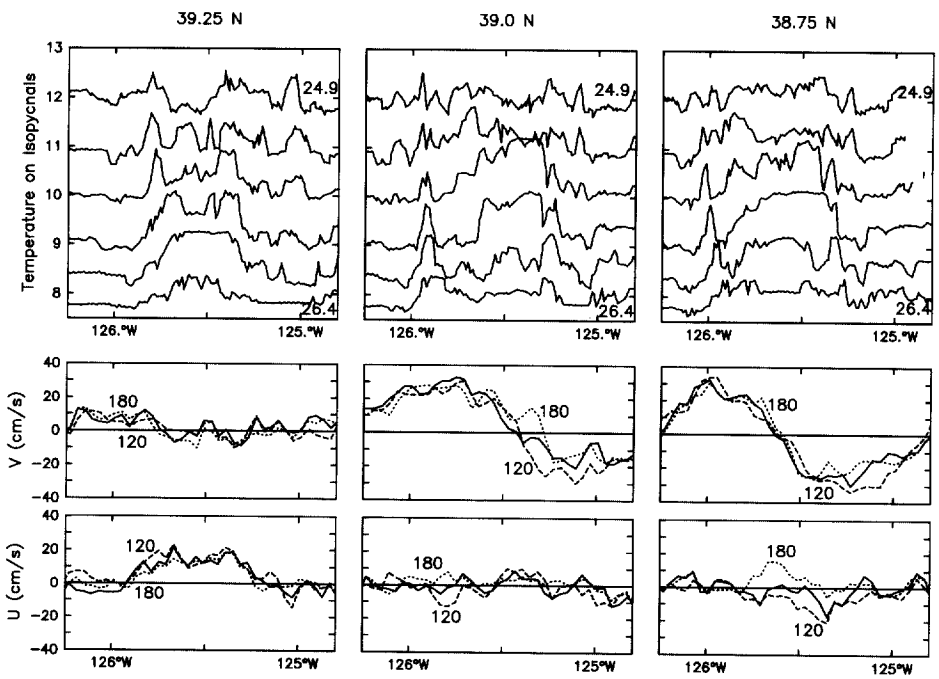

Fig. 17. Lateral profiles of temperature and velocity along the zonal sections at 39°15′, 39°00′ and 38°45′N in June. Upper panels shows temperature on selected isopycnals (24.9–26.4 $\mathrm{kg\,m^{-3}}$ at intervals of 0.3 $\mathrm{kg\,m^{-3}}$); lower panels show the northward current at 120, 150 and 180 m.

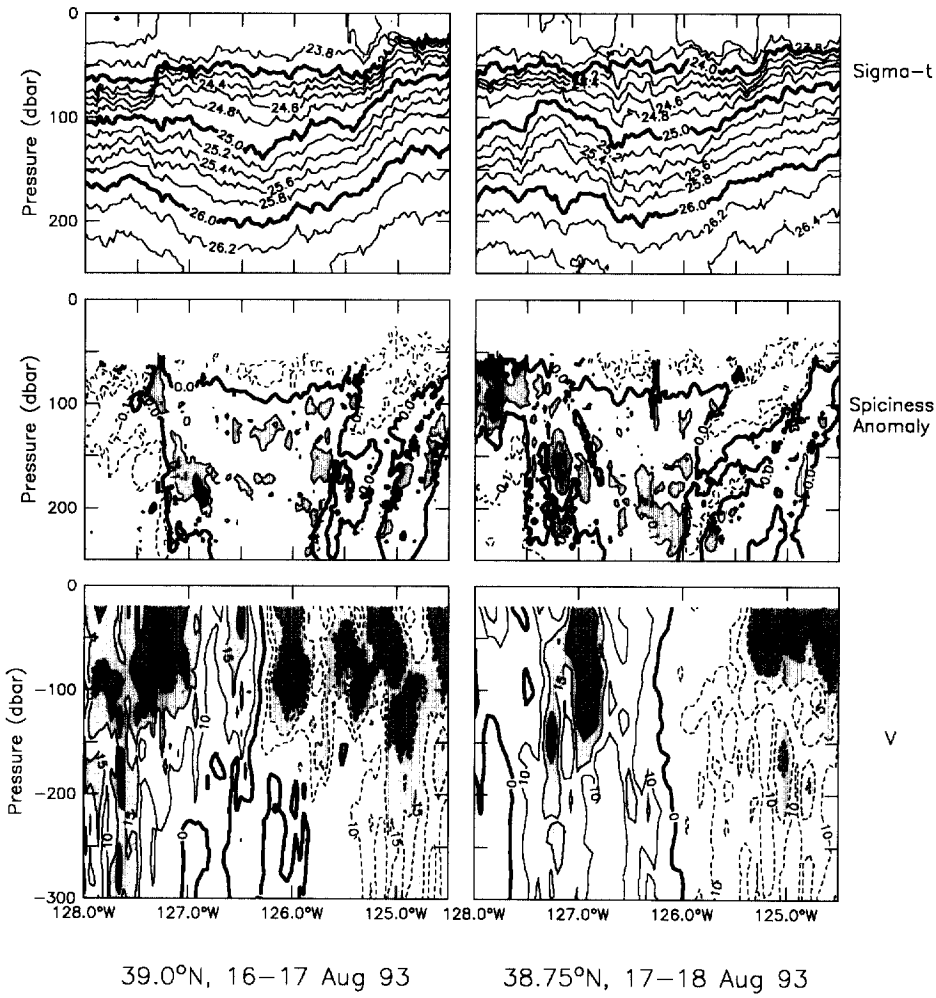

Fig. 18. Zonal sections through the northern warm-core eddy in August: density, spiciness anomaly and the northward component of velocity, along 39°00′N and 38°45′N, 16–18 June 1993. (Spiciness anomaly is the difference between actual spiciness and the northern average shown in Fig. 3).

isopycnal surfaces (Figs. 4–6), though vertical sections through it (Fig. 18) do show a large region of weakly positive spiciness anomalies bounded by anticyclonic currents. *T–S* diagrams (Fig. 19) show clearly that these water-mass anomalies are much weaker than those observed at the core of the northern eddy in June. If this is indeed the same eddy, its core waters were thoroughly mixed with its surroundings during the intervening seven weeks; such mixing could also account for the larger eddy diameter in August.

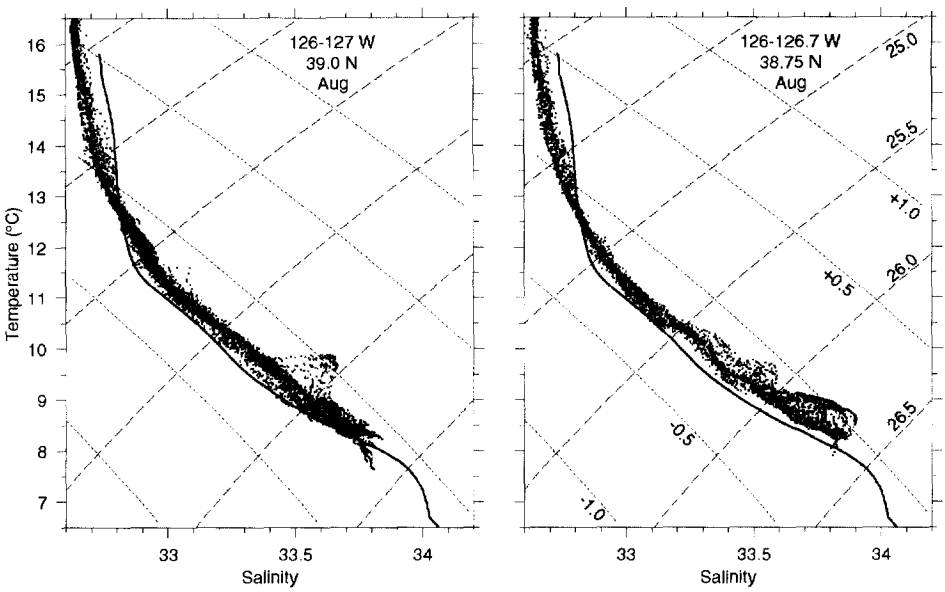

Fig. 19. *T–S* diagrams of Seasoar data near the core of the northern warm-core eddy in August. The heavy curve in each panel repeats the northern average from Fig. 3.

4.3. Other eddies

The 200 m ADCP data (Fig. 2b) show other eddies besides the two anticyclonic eddies described above, but these do not have distinctive water mass characteristics. One of these is the cyclonic eddy centered near 38°15′N, 125°00′W in June and 37°45′N, 127°15′W in August; this feature was tracked through much of the 1993 upwelling season, and migrated westward at a rate of about 5 cm s^{-1} after originating near Pt. Arena in May 1993 (Kosro et al., 1994, 1996; Chumbinho, 1994; Shearman et al., 1998). The anticyclonic eddy lying directly southeast of this anticyclone in August, at 37°20′N, 126°10′W was host to one of the subsurface floats ("Float 7") deployed by Garfield et al. (1997). Float 7 was deployed at a depth of 300 m at 37°55′N, 123°40′W over the continental slope off Pt. Reyes on 8 July 1993 (N. Garfield, personal communication); Fig. 2 shows a series of three anticyclonic eddies over the slope at the end of June, and the initial position and velocity of the float (17 cm s^{-1} westward) suggests it was deployed into the southern limb of the eddy that was centered at 38°30′N, 124°00′W at the end of June. After deployment, the float moved offshore at an average rate of 5 cm s^{-1}, about the same rate as the cyclonic eddy; we suggest that these two eddies traveled as a pair. The float surfaced on 4 September before leaving the eddy. The rapid migration and short life history are consistent with the absence of a strong water-mass signature for this eddy: the spiciness of waters near the slope

off Pt Reyes in late June is about the same as the spiciness in the core of this eddy in late August (Fig. 5).

The August survey shows one additional strong anticyclonic eddy, centered about 37°50′N, 124°10′W (Fig. 2b). This eddy shows little very shear in the upper 200 m, and does not appear as a feature in the dynamic topography (Fig. 1b), and the ADCP currents shows azimuthal velocities 30 cm s^{-1} at both 25 m (Fig. 1c) and 200 m (Fig. 2b). The eddy has a diameter of about 80 km. Water properties of the eddy core are similar to those of ambient waters, and there is no obvious spiciness signature. This eddy probably formed locally and recently, since the end of the June survey.

5. Conclusions

The high-resolution, large-area Seasoar surveys of the California Current region in the summer of 1993 have verified the existence of large-scale trends in the water-mass characteristics of the upper ocean, and provide new information on the characteristics of anticyclonic eddies in this region. The large-scale trends are consistent with those observed in the 1930s (Tibby, 1941), i.e. on an upper-ocean isopycnal surface, temperature and salinity tend to increase toward the equator and toward shore. The meridional trend is consistent with the large-scale gradient in climate: higher rainfall and less heating farther north. The zonal gradient is consistent with net poleward advection of more southerly waters through the California Undercurrent which flow north along the continental margin with a core-depth of 150–200 m.

Local extrema in the water-mass distributions along isopycnal surfaces tend to coincide with mesoscale features in the current field. As observed earlier in the Coastal Transition Zone study (Huyer et al., 1991; Kosro et al., 1991), minimum values of temperature, salinity and spiciness at shallow depths tend to coincide with the axis of the meandering, surface-intensified equatorward jet.

Local maxima in spiciness tend to coincide with subsurface anticyclonic eddies, which have a core-depth of about 150 m, about the same as the depth of the California Undercurrent. Isolated instances of such eddies have been observed earlier: near Pt. Conception in 1985 (Simpson and Lynn, 1990), and near Pt. Arena in 1987 (Kosro et al., 1991). One anticyclonic eddy, observed at about 36°20′N, 125°15′W in June, had a subsurface lens of very uniform water at its core that was about 1°C warmer and 0.3 psu more saline than surrounding waters of the same density; this eddy probably originated over the continental margin during the preceding winter. This eddy is reminiscent of the high-salinity meddies observed in the eastern North Atlantic, though its diameter is larger and its core depth much shallower. Another anticyclonic eddy, observed at about 39°00′N, 125°30′W in June and 39°00′N, 126°30′W in August, had a very patchy core in June that became more homogeneous by August. This eddy probably originated over the continental margin in early spring. Additional anticyclonic eddies without a strong water-mass signature were observed in both surveys, and these also appeared to have a local and recent origin over the continental margin. Some of our anticyclonic eddies definitely had a subsurface core and strong vertical

shear, and some were nearly barotropic with very little vertical shear between 25 and 200 m. Migration rates of 1–5 cm s^{-1}, estimated from the observed position and the presumed time of origin, were consistent with those obtained from recent deployments of subsurface RAFOS floats (Garfield et al., 1998). Garfield et al. (1998) concluded that their anticyclonic RAFOS trajectories sampled submesoscale coherent vortices. We believe we sampled the same kind of feature; if so, our data indicate that the float trajectories (at 300 m) lay well below the core-depth ($\sim$ 150 m). All of the eddies we observed were of diameter > 50 km which is larger than the baroclinic radius of deformation. The fine-resolution hydrographic surveys have provided a more complete view of the eddy structure and characteristics, and support the view that most or all eddies in the California Current are generated inshore and migrate offshore.

Acknowledgements

We are deeply indebted to Wecoma's Marine Technicians (Marc Willis, Brian Wendler, Mike Hill and Tim Holt) for the successful operation of the Seasoar system in this challenging environment, and to Robert O'Malley and Jane Fleischbein for archiving and processing the data and assistance in analysis. We are also grateful to every cruise participant, and to the officers and crew of Wecoma. Discussions with our EBC colleagues contributed to the survey design, and more recently to interpreting the results: we are especially grateful to Teri Chereskin, Curt Collins, Toby Garfield, and Ron Lynn. This work was supported by the Office of Naval Research through Grants N00014-92J1348, N00014-92J1357 and by an AASERT Grant N00014-93-0730.

References

Abbott, M.R., Letelier, R.M., Barksdale, B., 1996. Lagrangian statistics as observed by near-surface bio-optical drifters in the California Current. Abstract only. EOS, Transactions of American Geophysical Union 76(3) (Suppl. OS131), 1996.

Allen, J.S., 1973. Upwelling and coastal jets in a continuously stratified ocean. Journal of Physical Oceanography 3, 245–257.

Allen, J.S., Newberger, P.A., Federiuk, J., 1995. Upwelling circulation on the Oregon continental shelf, Part I: Response to idealized forcing. Journal of Physical Oceanography 25, 1843–1866.

Armi, L., Hebert, D., Oakey, N., Price, J.F., Richardson, P.L., Rossby, T.H., Ruddick, B., 1989. Two years in the life of a Mediterranean salt lens. Journal of Physical Oceanography 19, 354–370.

Blanton, J., Pattullo, J.G., 1970. The subsurface boundary between subarctic Pacific water and Pacific equatorial water in the transition zone off southern California. Limnology Oceanography 15, 606–614.

Brainerd, K.E., Gregg, M.C., 1995. Surface mixed and mixing layer depths. Deep-Sea Research 42, 1521–1543.

Chelton, D.B., Bernstein, R.L., Bratkovitch, A., Kosro, P.M., 1987. The central California coastal circulation study. EOS, Transactions, American Geophysical Union 68, 12–13.

Chereskin, T.K., Firing, E., Gast, J.A., 1989. Identifying and screening filter skew and noise bias in Acoustic Doppler Current Profiler measurements. Journal of Atmospheric and Oceanic Technology 6, 1040–1054.

Chumbinho, R.P., 1994. Kinematics and dynamics of a cyclonic eddy off Pt. Arena, California. Ph.D. Dissertation, Naval Postgraduate School, Monterey, CA, 79pp.

Collins, C.A., Garfield, N., Paquette, R.G., Carter, E., 1996. Lagrangian measurement of subsurface poleward flow between 38°N and 43°N along the west coat of the United States during summer 1993. Geophysical Research Letters 23, 2461–2464.

Cowles, T.J., Desiderio, R.A., Potter, N., Moore, C., 1991. Steep gradients in phytoplankton biomass in eastern boundary currents: Observations with a multi-excitation spectral fluorometer. Abstract only. Transactions of American Geophysical Union, EOS 75(3), (Suppl.) 141.

Flament, P., 1986. Finestructure and subduction associated with upwelling filaments, Ph. D. Dissertation, University of California San Diego.

Fleischbein, J., Gilbert, W.E., Schramm, R., Huyer, A., 1981. CTD observations off Oregon and California, 5–17 February 1981. School of Oceanography, Oregon State University Data Report 90, Ref. 81–16. 122 pp.

Fofonoff, N.P., Millard, R.C. Jr., 1983. Algorithms for computation of fundamental properties of seawater. Unesco Technical Papers in Marine Science vol. 44, 53 pp.

Fofonoff, N.P., Tabata, S., 1966. Variability of oceanographic conditions between Ocean Station P and Swiftsure Bank off the Pacific coast of Canada. Journal of Fisheries Research Board of Canada 23, 825–868.

Freitag, H.P., Halpern, D., 1981. Hydrographic observations off northern California during May 1977. Journal of Geophysical Research 86, 4248–4252.

Garfield, N., Collins, C.A., Paquette, R.G., Carter, E., 1998. Lagrangian Exploration of the California Undercurrent, 1992–1995. Journal of Physical Oceanography, in press.

Halpern, D., Smith, R.L., Reed, R.K., 1978. On the California Undercurrent over the continental slope off Oregon. Journal of Geophysical Research 83, 1366–1372.

Hastenrath, S., Lamb, P.J., 1977. Climatic Atlas of the Tropical Atlantic and Eastern Pacific Oceans. University of Wisconsin Press, Madison.

Hastenrath, S., Lamb, P.J., 1978. Heat Budget Atlas of the Tropical Atlantic and Eastern Pacific Oceans. University of Wisconsin Press, Madison, 90 pp.

Hickey, B.M., 1979. The California Current system – hypotheses and facts. Progress in Oceanography 8, 191–279.

Huntley, M.E., Zhou, M., Nordhausen, W., 1995. Mesoscale distribution of zooplankton in the California Current in late spring, observed by Optical Plankton Counter. Journal of Marine Research 53, 647–674.

Huyer, A., 1983. Coastal Upwelling in the California current system. Progress in Oceanography 12, 259–284.

Huyer, A., 1984. Hydrographic observations along the CODE Central Line off northern California, 1981. Journal of Physical Oceanography 14, 1647–1658.

Huyer, A., 1990. Shelf circulation. In: Le Mehaute, B., Hanes, D.M. (Eds.) The Sea, vol. 9: Ocean Engineering Science. Wiley, New York, pp. 423–466.

Huyer, A., Kosro, P.M., Fleischbein, J., Ramp, S.R., Stanton, T., Washburn, L., Chavez, F.P., Cowles, T., Pierce, S.D., Smith, R.L., 1991. Currents and water masses of the Coastal Transition Zone off Northern California, June to August 1988. Journal of Geophysical Research 96, 14,809–14,831.

Huyer, A., Kosro, P.M., Lentz, S., Beardsley, R.C., 1989. Poleward flow in the California Current system. In: Neshyba, S.J., Mooers, C.N.K., Smith, R.L., Barber, R.T. (Eds.), Poleward Flows Along Eastern Ocean Boundaries, Coastal and Estuarine Studies, vol. 34. Springer, Berlin, pp. 142–156.

Huyer, A., Smith, R.L., Hickey, B.M., 1984. Observations of a warm-core eddy off Oregon, January to March 1978. Deep-Sea Research 31, 97–117.

Kosro, P.M., 1985. Shipboard acoustic current profiling during the Coastal Ocean Dynamics Experiment. Ph.D. Thesis, SIO Ref. 85-8, 119 pp., Scripps Inst. of Oceanogr., La Jolla, Calif.

Kosro, P.M., Barth, J.A., Fleischbein, J., Huyer, A., O'Malley, R., Shearman, R.K., Smith, R.L., 1995. Seasoar and CTD Observations during EBC Cruises W9306A and W9308B, June to September 1993, College of Ocean. and Atmospheric Science Oregon State University, Data Report 160, Ref. 95-2, 393 pp.

Kosro, P.M., Huyer, A., 1986. CTD and velocity surveys of seaward jets off northern California, July 1981 and 1982. Journal of Geophysical Research 91, 7680–7690.

Kosro, P.M., Huyer, A., Ramp, S.R., Smith, R.L., Chavez, F.P., Cowles, T.J., Abbott, M.R., Strub, P.T., Barber, R.T., Jessen, P., Small, L.F., 1991. The structure of the transition zone between coastal waters and the open ocean off northern California, winter and spring 1987. Journal of Geophysical Research 96, 14,707–14,730.

Kosro, P.M., Huyer, A., Barth, J., Smith, R.L., Strub, P.T., 1994. Eddies in the California Current region off northern California from satellite and Seasoar-ADCP measurement. Abstract only. EOS, Transactions of American Geophysical Union 75(3), (Suppl.) 140.

Kosro, P.M., Huyer, A., Barth, J., Smith, R.L., Pierce, S.D., Strub, P.T., 1996. Studies of the California Current and Undercurrent. Paper Presented at the Benguela Meeting, November 1996.

Limeburner, R., Beardsley, R.C., Brink, K.H., 1994. Lagrangian measurements of eddy characteristics in the California Current. Abstract only. EOS, Transactions of American Geophysical Union 75(3), (Suppl.), 151.

Lynn, R.J., Simpson, J.J., 1987. The California Current System: The seasonal variability of physical characteristics. Journal of Geophysical Research 92, 12,947–12,966.

Lynn, R.J., Simpson, J.J., 1990. The flow of the undercurrent over the continental borderland off southern California. Journal of Geophysical Research 95, 12,995–13,008.

Lynn, R.J., Schwing, F.B., Hayward, T.L., 1995. The effect of the 1991–1993 ENSO on the California Current system. CalCOFI Report 36, 57–71.

Nelson, C.S., Husby, D.M., 1983. Climatology of surface heat fluxes over the California Current region. U.S. Dept. of Commerce., NOAA Technical Report NMFS SSRF-763, 155 pp.

Pierce, S.D., Allen, J.S., Walstad, L.J., 1991. Dynamics of the coastal transition zone jet: Part I, Linear stability analysis. Journal of Geophysical Research 96, 14,979–14,993.

Pollard, R., Read, J., 1989. A method for calibration shipmounted acoustic Doppler profiles and the limitations of gyro compasses. Journal of Oceanic and Atmospheric Technology 6, 859–865.

Prater, M.D., Sanford, T.B., 1994. A meddy off Cape St. Vincent. Part I: description. Journal of Physical Oceanography 24, 1572–1586.

Richardson, P.L., Walsh, D., Armi, L., Schroder, M., Price, J.F., 1989. Tracking three meddies with SOFAR floats. Journal of Physical Oceanography 19, 371–383.

Shearman, R.K., Barth, J.A., Kosro, P.M., 1997. Diagnosis of the three-dimensional circulation associated with mesoscale motion in the California Current. Journal of Physical Oceanography, in press.

Simpson, J.J., Lynn, R.J., 1990. A mesoscale eddy dipole in the offshore California Current. Journal of Geophysical Research 95, 13009–13022.

Smith, R.L., 1992. Coastal upwelling in the modern ocean. In: Summerhayes, C.P., Prell, W.L., Emeis, K.C. (Eds.), Upwelling Systems: Evolution Since the Early Miocene, Geological Society Special Publication No 64, London, pp. 9–28.

Smith, R.L., Pierce, S.D., Barth, J.A., Kosro, P.M., Wilson, C., 1996a. Extensive observations of the poleward undercurrent along the continental margin off California, Oregon and Washington. Abstract only. EOS, Transactions American Geophysical Union 77(3), (Suppl.), OS131.

Smith, R.L., Barth, J.A., Huyer, A., Kosro, P.M., Pierce, S.D., 1996b. Alongshore advection in coastal upwelling regions: the continuity of the equatorward surface jet and the poleward undercurrent. Abstract of paper presented at meeting of The Oceanography Society, Amsterdam, July 1996.

Strub, P.T., Kosro, P.M., Huyer, A., and CTZ Collaborators, 1991. The nature of the cold filaments in the California Current system. Journal of Geophysical Research 96, 14,743–14,768.

Tabata, S., 1975. The general circulation of the Pacific Ocean and a brief account of the Oceanographic structure of the North Pacific Ocean, Part I – Circulation and volume transports. Atmosphere 13, 133–168.

Tabata, S., 1976. The general circulation of the Pacific Ocean and a brief account of the Oceanographic structure of the North Pacific Ocean, Part II – Thermal regime and influence on climate. Atmosphere 14, 1–27.

Tibby, R.B., 1941. The water masses off the west coast of North America. Journal of Marine Research 4, 112–121.

Walstad, L.J., Allen, J.S., Kosro, P.M., Huyer, A., 1991. Dynamics of the Coastal Transition Zone in 1987 through data assimilation studies. Journal of Geophysical Research 96, 14,959–14,977.

Wooster, W.S., Reid, J.L., 1963. Eastern boundary currents. In: Hill, M.N. (Ed.), The Sea, vol. 2. Wiley Interscience, New York, pp. 253–280.

Wyllie, J.G., 1966. Geostrophic flow of the California Current at the surface and at 200 meters. California Cooperative Oceanic Fisheries Investigations Atlas 4. State of California Marine Research Committee.